**Chapter 5**. **Estimating Stress Heterogeneity and Background Stress in the Real Earth**

Ultimately, we wish to estimate stress heterogeneity parameters in the real Earth by comparing our simulations to real focal mechanism data. Very little is known about the parameters of stress heterogeneity in the Earth, so this is an exciting topic of investigation. At the same time we have to keep in mind that there are limitations to our ability to test this, because of all the simplifying assumptions incorporated into our 3D numerical models. For example, when generating the three principal stresses ($\sigma_1$, $\sigma_2$ and $\sigma_3$), we start with Gaussian random noise in 3D and then smooth it with a fractal filter. In the real Earth, a Weibull distribution may be more appropriate. While spatial smoothing using a fractal filter may simply describe the statistics of our simulations, there is no guarantee that the real Earth's spatial stress heterogeneity varies exactly in a fractal manner. Then when we generate the actual failures, they are point failures, not finite dislocations, and we do not update the stress field. We also use a plastic yield criterion to determine failures, which means we do not allow the possibility of slip on pre-existing faults. The lack of pre-existing faults means that the spatial clustering of our focal mechanisms tends to occur in 3D clouds rather than lineations or planes; whereas, in the real Earth, seismicity often occurs on lineations or planes due to preexisting faults and fracture zones. Therefore, any conclusions derived from comparing our simulations to real data are meant to yield an initial estimate to be tested and refined by better future techniques.

The two stress heterogeneity parameters we wish to estimate are $\alpha$, the degree of spatial smoothing, and $HR$, which describes the relative magnitudes of the spatial heterogeneity and the spatial mean. We will also have to estimate how much model noise

(as opposed to stress heterogeneity) to add to our simulated focal mechanisms to accurately compare them with real focal mechanisms; i.e., there is a mechanism uncertainty/error in the generation of real focal mechanism data that has to be taken into account if we wish to compare our simulations to real data. We will also show that the failure threshold, $\frac{2}{3}\tau_0^2$, can be an important factor as well.

To estimate $\alpha$, $HR$, and the model noise, we compare our simulations to a plot by Hardebeck [in review, 2006], that plots the average angular difference between pairs of focal mechanisms as a function of distance between the pairs for three different regions (Figures 5.1–5.2). Figure 5.1 is a modified map from Hardebeck [in review, 2006] that shows the regions in which she computed the average angular difference between pairs of focal mechanisms and the two regions we numerically model. Figure 5.2, another modified plot from Hardebeck [in review, 2006], shows the average angular difference as a function of distance for two of the regions she studied. According to Hardebeck, for length scales < ~ 2 km the average focal mechanism variation could be explained purely by uncertainty in the focal mechanism orientations. However, as the length scale increases, the average focal mechanism variation also increases, which we will show is consistent with smoothed heterogeneous stress similar to our simulations. We will show that:

- The minimum average angular difference between focal mechanisms in Figure 5.2 can be used to estimate how much noise should be added to our simulated data. One assumes the stress is uniform at those small distances, and the minimum average angular difference is due purely to model noise.

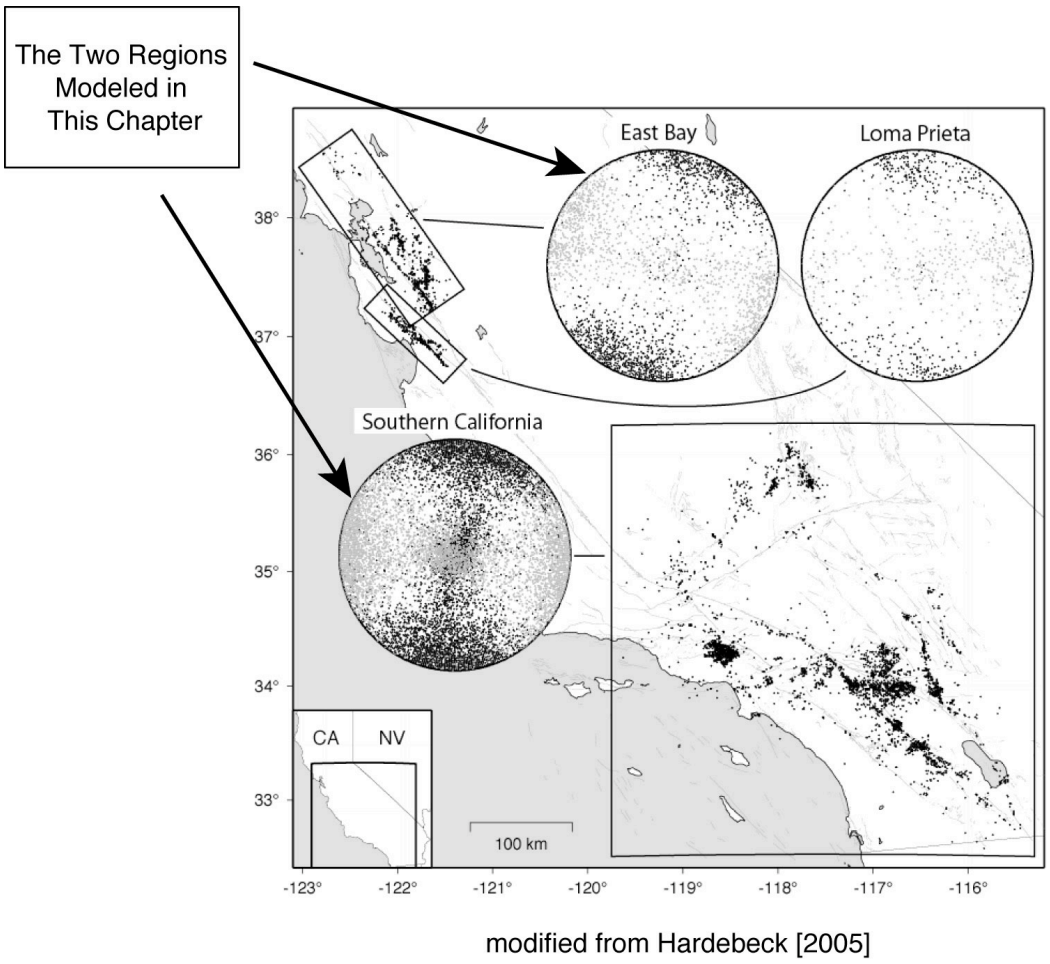


**Figure 5.1.** *A modified map of the three regions Hardebeck [in review, 2006] studied and P-T plots of the mechanisms used to calculate average focal mechanism difference as a function of length as seen in Figure 5.2. In this chapter we model two of the three regions, Southern California and East Bay. The P axes in the stereonet plot are the darker-shaded points. They are slightly rotated from a North-South trend. The T axes are the ligher-shaded points, slightly rotated from an East-West trend.*

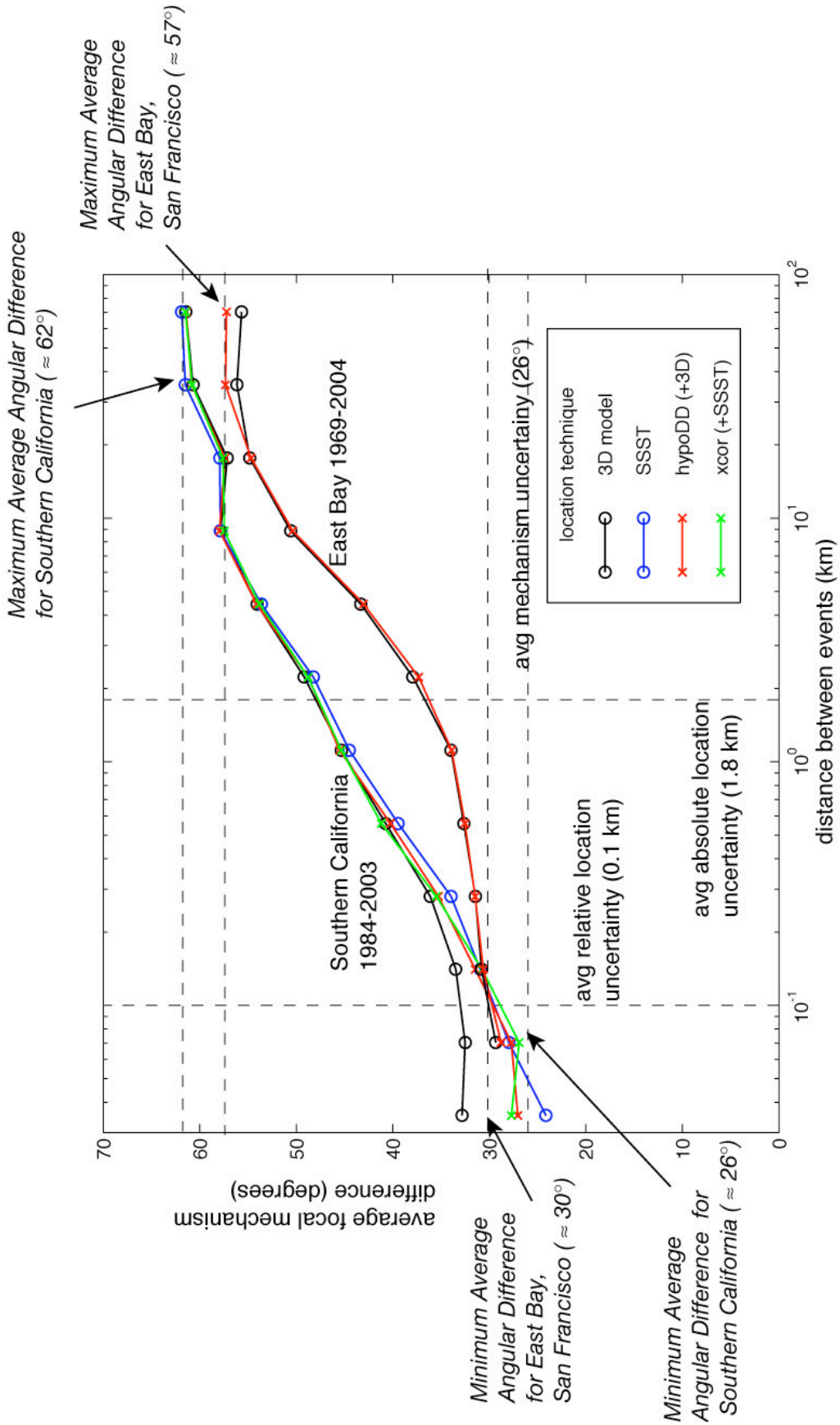
Maximum Average Angular Difference for Southern California ( ≈ 62°)
Maximum Average Angular Difference for East Bay, San Francisco ( ≈ 57°)
East Bay 1969-2004
Southern California 1984-2003
avg mechanism uncertainty (26°)
avg relative location uncertainty (0.1 km)
avg absolute location uncertainty (1.8 km)
location technique
3D model
SSST
hypoDD (+3D)
xcor (+SSST)
average focal mechanism difference (degrees)
distance between events (km)
Minimum Average Angular Difference for East Bay, San Francisco ( ≈ 30°)
Minimum Average Angular Difference for Southern California ( ≈ 26°)

**Figure 5.2.** *Average focal mechanism difference between pairs of focal mechanisms as a function of distance between the pairs, for two regions, Southern California and East Bay, San Francisco, modified from Hardebeck [in review, 2006]. At first glance, we can begin pulling out numbers that will help us parameterize the heterogeneity. If one assumes that the stress is approximately spatially uniform where the curve levels out for small scales on the left, then any non-zero average focal mechanism difference must be due purely to noise. When we numerically simulate the model noise, we will find how to reproduce a ~ 26° average focal mechanism difference or ~ 30° average focal mechanism difference for uniform focal mechanisms with noise added. The increasing average focal mechanism difference as a function of length is compatible with a spatially smoothed heterogeneous crust as we will show later. The maximum average focal mechanism difference should occur at the point where the points are far enough away that there is no longer significant spatial correlation due to smoothing. This curve flattens out to what one would expect for completely random, uncorrelated heterogeneous noise to produce; hence, the amplitude of this maximum will depend on the amplitude of the heterogeneity,* $HR$*, and of course the noise level. For Southern California, it flattens out to ~62° and for East Bay, San Francisco to ~57°. We will use these values to help us set the* $HR$ *parameter. Last, the slope of the lines will help us set the spatial smoothing parameter,* $\alpha$*. If* $\alpha = 0.0$*, Southern California would be a straight line at ~ 62°, and East Bay would be a straight line at ~ 57°. Instead, it appears that there is spatial smoothing to the heterogeneity. In general, the steeper the slope the more smoothed the heterogeneity; therefore, we would expect a larger value of* $\alpha$ *for East Bay, San Francisco than for Southern California.*

- Once we have an estimate of the model noise, the maximum average angular difference between focal mechanisms in Figure 5.2 can be used to estimate the heterogeneity ratio, $HR$. In Figure 5.2, the average angular difference increases as a function of distance then levels out at some maximum. When we produce similar plots from our numerical simulations using the three-component method from Chapter 4, we find that ratio of heterogeneity to $\sigma'_B$, $HR$, determines this maximum. If $HR \to \infty$, the average angular difference saturates at approximately 75°, whereas if $HR \approx 0$, the maximum is simply at the noise level because all the focal mechanisms have approximately the same orientations, and the only source of variation is noise.
- Last, the slope of the plots in Figure 5.1 will enable us to estimate the degree of spatial smoothness in the heterogeneity, the parameter, $\alpha$. For example, if $\alpha = 0.0$, there is no spatial correlation between focal mechanisms, and each pair of focal mechanisms is equally uncorrelated regardless of spatial separation; hence, one would expect a flat line at the maximum angular difference associated with $HR$. As $\alpha$ increases, the slope will also increase because the stress tensors for closely spaced points are becoming increasing similar.

**Estimating the Model Noise in Real Data Due to Focal Mechanism Orientation Uncertainty**

In Figure 5.2, modified from Hardebeck [2006], the average angular difference reaches a minimum at ≈ 26° for the Southern California region and ≈ 30° for the East Bay region. We will assume that these minimum angular differences are purely an effect of

model noise, and that the stress itself is approximately uniform at those distances. We can simulate this by creating a set of focal mechanisms with the same orientations, adding Gaussian noise with different mean deviations, calculating the average angular difference between pairs of focal mechanisms, and eventually finding a level of Gaussian noise that duplicates the 26° and 30° minima. We add the model noise using the quaternion mathematics shown in Chapter 3, where we:

- Generate completely random unit quaternions.
- Convert them into our three rotation parameters, $(\omega,[\theta,\phi])$.
- Keep the random rotation axes, $[\theta,\phi]$, and combine them with a new $\omega'$.
- The new $\omega'$ is generated using Gaussian white noise with a mean of zero and some specified mean deviation. The mean deviation is the parameter we need to vary to match it with the average angular difference of $\approx 26°$.
- Convert $(\omega',[\theta,\phi])$ into unit quaternions and use quaternion multiplication to add these random rotations to the set of uniform focal mechanisms.
- Use these unit quaternions to transform the original focal mechanism and derive the new strike, dip, and rake, $(\Theta,\delta,\lambda)$ or P and T axes.

Figure 5.3 shows what P-T axes would look like for different levels of model noise starting with completely homogeneous stress (all the focal mechanisms have the same orientation before adding the noise). We show a total of 2,000 focal mechanisms on each plot. On the left, we use the Southern San Andreas Fault background stress tensor, $\boldsymbol{\sigma}'_{B_1}$, that is applied to the simulations in Chapter 4, and on the right, we use the San Gabriel Mountains background stress tensor, $\boldsymbol{\sigma}'_{B_2}$, also from our simulations in

Chapter 4. We add noise onto these background stresses for $\omega$ mean deviations of 10°, 20° and 30°, where the mean noise deviation is defined as,

$$MeanDeviation = \frac{1}{N}\sum_{i=1}^{N}|\omega_i|. \tag{5.1}$$

When we try to estimate the model noise parameter for real data, we find that an $\omega$ mean deviation of ~ 17° yields an ~ 26° minimum angular difference as seen in Hardebeck [2006] for the Southern California region. For the East San Francisco Bay region, there may be a slightly larger minimum average angular difference, ~30°, which can be modeled with an $\omega$ mean deviation of ~ 20°. Figure 5.4 shows the average angular difference as a function of distance for uniform focal mechanisms that have had random Gaussian noise added with ~17° and ~ 20° mean deviations. They are approximately straight lines because we have simply added spatially uncorrelated noise to all points.

Southern San Andreas $\sigma_B$, Mean Deviaton = 10 Degrees

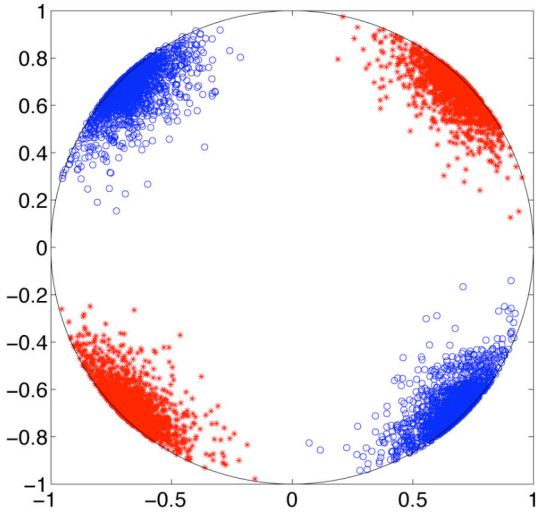

San Gabriel Mountains $\sigma_B$, Mean Deviaton = 10 Degrees

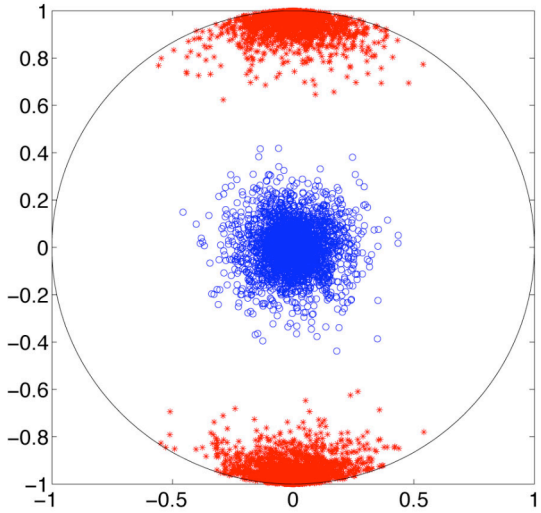

Southern San Andreas $\sigma_B$, Mean Deviaton = 20 Degrees

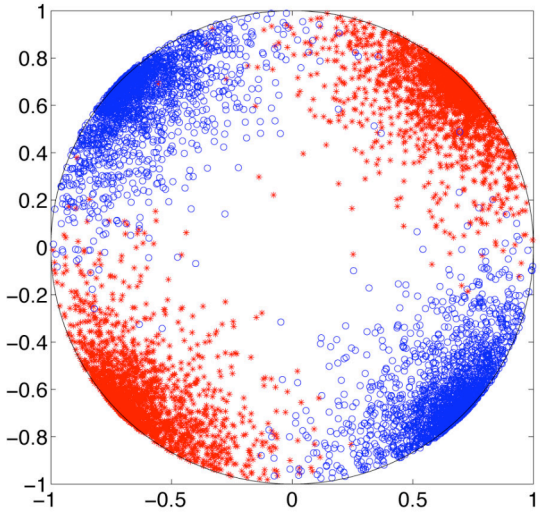

San Gabriel Mountains $\sigma_B$, Mean Deviaton = 20 Degrees

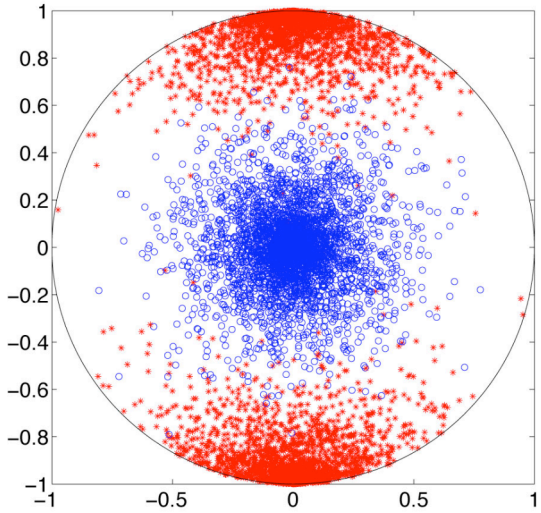

Southern San Andreas $\sigma_B$, Mean Deviaton = 30 Degrees

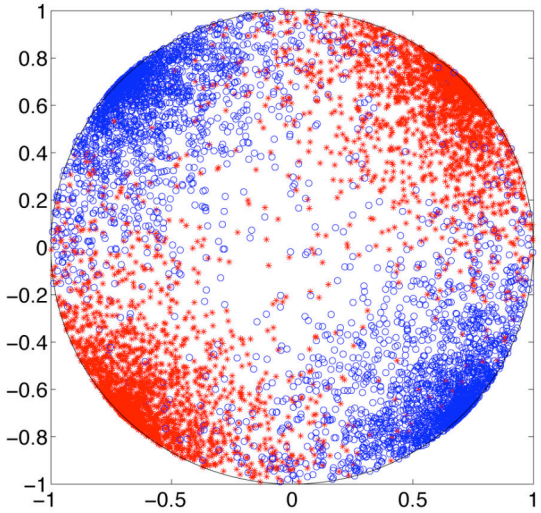

San Gabriel Mountains $\sigma_B$, Mean Deviaton = 30 Degrees

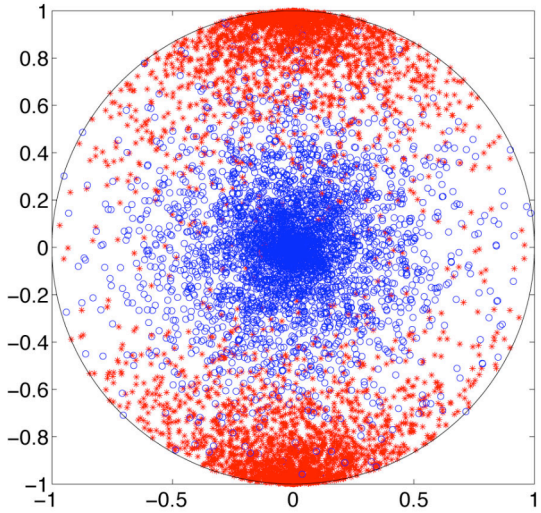

**Figure 5.3.** *P-T plots of noise. The P axes are plotted with red asterisks, and the T axes are plotted with blue open circles. For each plot, 2,000 focal mechanisms of the same orientation are given random rotations; therefore, any scatter in the P-T axes is due purely to model noise, not stress heterogeneity. On the left, we start with the Southern San Andreas Fault background stress tensor,* $\boldsymbol{\sigma}'_{B_1}$*, used in our simulations for Chapter 4. On the right we start with the San Gabriel Mountains background stress tensor,* $\boldsymbol{\sigma}'_{B_2}$*, also used in our Chapter 4 simulations. The top row plots the noise generated from random Gaussian angle rotations,* $\omega$*, with mean deviation = 10°. The center row has a mean deviation of 20°, and the bottom row has a mean deviation of 30°. Mean deviations of* $\approx$ *17– 20° produce model noise that best matches real data, similar to the center row.*

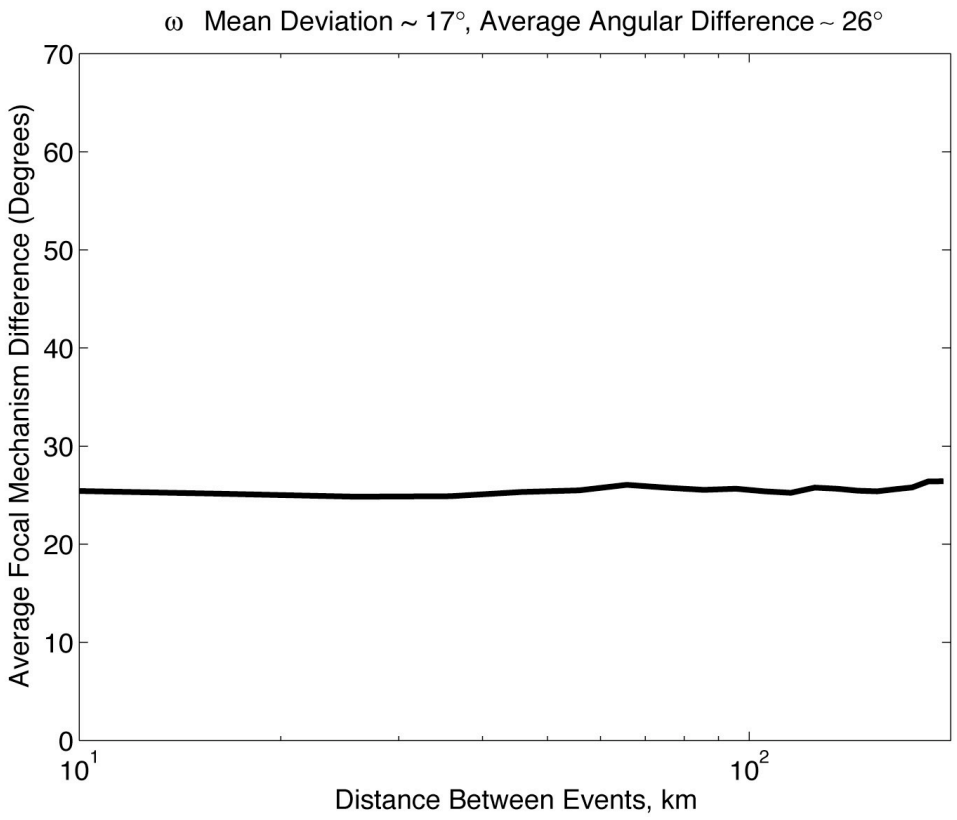
ω Mean Deviation ~ 17°, Average Angular Difference ~ 26°
Average Focal Mechanism Difference (Degrees)
0
10
20
30
40
50
60
70
$10^1$
$10^2$
Distance Between Events, km

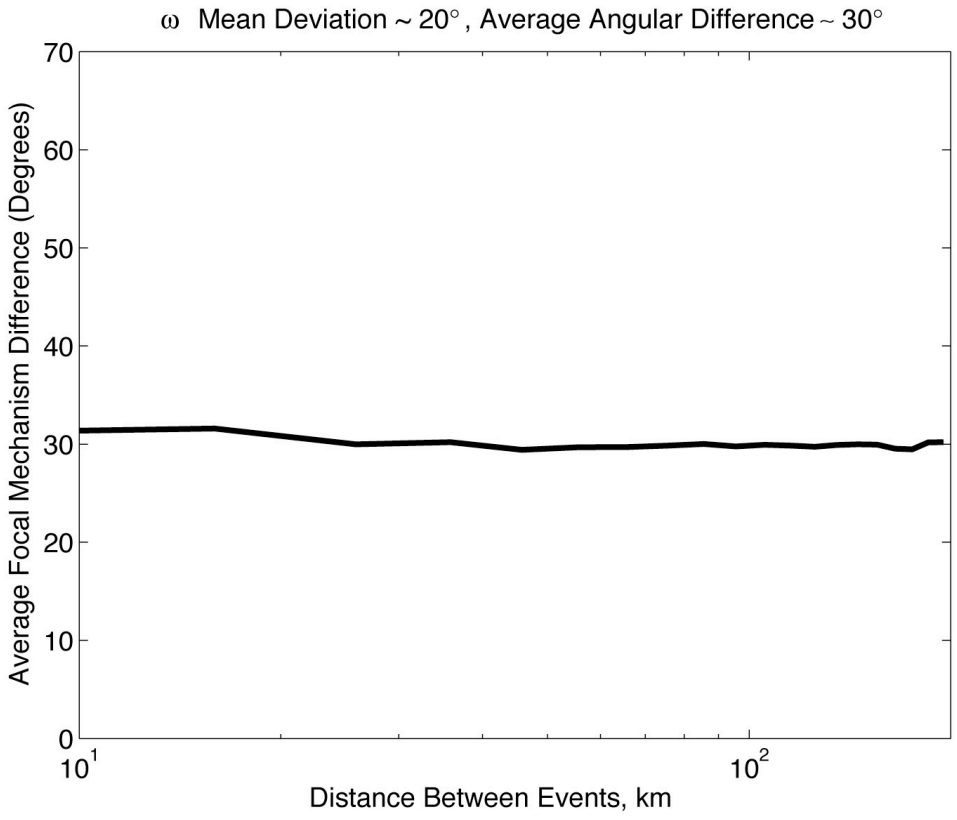
ω Mean Deviation ~ 20° , Average Angular Difference ~ 30°
Average Focal Mechanism Difference (Degrees)
0
10
20
30
40
50
60
70
$10^1$
$10^2$
Distance Between Events, km

**Figure 5.4.** *We start with 500 uniformly oriented focal mechanisms and add random Gaussian noise with a mean deviation of ~17° for the top plot and ~20° for the bottom plot. Then we calculate the average focal mechanism difference as a function of distance. It yields approximately straight lines at ~26° for the top plot and ~ 30° for the bottom plot. This matches the minimum values for Southern California and East Bay, San Francisco respectively in Figure 5.2; therefore, we now know how much model noise to add to our simulations to adequately represent focal mechanism uncertainties.*

**Table 5.1.** Misfit Statistics for Synthetic Simulations With Gaussian Noise Added

| Mean Deviation for Simulations | Mean of the Misfit Angle | Standard Deviation of the Misfit Angle |
|---|---|---|
| Southern San Andreas, 17° | 10.0944° | 13.7134 |
| San Gabriel Mountains, 17° | 10.1084° | 13.6266 |
| Southern San Andreas, 20° | 12.9599° | 18.7245 |
| San Gabriel Mountains, 20° | 12.9816° | 18.7866 |
| Southern San Andreas, 26° | 20.0672 | 29.0822 |
| San Gabriel Mountains, 26° | 20.0372 | 29.0511 |

*For each row in the table, we generate 50 sets of 1,000 noisy uniform focal mechanisms and apply Andy Michael's program, "slick" [Michael, 1984; 1987]. Each inversion produces a mean misfit, and we average this parameter over the fifty sets. We start with two different uniform orientations, which we call the "Southern San Andreas Fault" and "San Gabriel Mountains" from Chapter 4, and apply Gaussian random noise with mean deviations of ~ 17° and ~20°. As the mean deviation of the model noise applied increases, so does the mean misfit angle from the inversions. Even though the Southern San Andreas and San Gabriel Mountains background stresses provide significantly different baseline orientations upon which model noise has been added, the mean misfit angles are nearly identical for these two types of simulations.*

The relationships between mean deviation, standard deviation, and average deviation between points for a 1D Gaussian distribution in 1D Cartesian coordinates, can shed some light on our statistics. We know that for 1D Gaussians,

$$\text{Mean Deviation} = \sqrt{\frac{2}{\pi}}\ \text{Standard Deviation} \tag{5.2}$$

and

$$\text{Average Deviation Between Points} = \sqrt{2}\ \text{Standard Deviation.} \tag{5.3}$$

Consequently,

$$\text{Average Deviation Between Points} = \sqrt{\pi}\ \text{Mean Deviation.} \tag{5.4}$$

For 1D Gaussian distributions, if the Mean Deviation is 17, one would expect an Average Deviation Between Points of 30.13, and if the Mean Deviation is 20, one would expect an Average Deviation Between Points of 35.45. Our average angular differences of 26° and 30° are slightly smaller than one might expect for Mean Deviations of 17° and 20° using the above 1D statistics, but this most likely occurs because we are calculating the minimum angles between focal mechanisms using three dimensions instead of one. The statistics for 1D Cartesian Gaussians and our Gaussian angle, $\omega$, do not have a one-to-one correspondence.

In Table 5.1 we show the statistics from applying a focal mechanism inversion program [*Michael*, 1984; 1987] to our noisy uniform focal mechanisms. For each row in the table, we generate 50 sets of 1,000 noisy uniform focal mechanisms and apply the program, "slick." The program attempts to find a best-fit spatially uniform stress field that minimizes the angular misfits between the actual slip vectors and the model slip vectors from a uniform stress field. One generated parameter is the mean angular misfit,

which we show in Table 5.1 for our homogeneous, but noisy focal mechanisms. This parameter is important because the mean angular misfit will increase as the stress heterogeneity increases. Therefore, one way of estimating the heterogeneity of a region is to

- Apply a focal mechanism inversion to the focal mechanisms in the region.
- Estimate the model noise in the focal mechanisms, due to uncertainty in focal mechanism orientations.
- Run several simulations of the region with 3D stress heterogeneity of different heterogeneous amplitudes, $HR$.
- Add the estimated model noise to the synthetic focal mechanisms.
- Apply the focal mechanism inversion to the noisy focal mechanisms.
- Compare the mean angular misfit from the real data in the region to the set of simulations with different levels of heterogeneity and find which $HR$ produces a mean angular misfit that best matches the real data.

**Estimating Stress Heterogeneity Parameters**

We calculate the average focal mechanism difference as a function of distance for our simulations. Note, we are using the three-component method from Chapter 4 that calculates the minimum angle between focal mechanisms using only angular information. The stress ratio, $R$, is not taken into account. This is true for Figures 5.5–5.8. Taking the first 2,000 failures from our 3D numerical simulations we calculate the angular difference between each pair of synthetic focal mechanisms and average those values as a function of pair distance. Using the $\omega$ mean deviation levels of 17° and 20° to model

noise, we vary the two heterogeneity parameters, $\alpha$ and $HR$, until we find curves that approximately match Hardebeck's [2006] plots for Southern California and East Bay, San Francisco. In Figures 5.5–5.7, we first show the effect of varying our three parameters, $\alpha$, $HR$, and the mean deviation of the $\omega$ noise. Then in Figure 5.8, we plot our best fits on top of Hardebeck's data for Southern California and East Bay, San Francisco.

The curves for Figures 5.5–5.7 are averaged over 4 different 3D simulations, using the same random seed for each $\alpha$. Our final curves in Figure 5.8 use a minimum of five different random seeds, i.e, five different filtered 3D heterogeneous grids for each curve, and six different simulations per random seed, for a total of at least 30 different simulations for Southern California and 30 different simulations for the East Bay, San Francisco. We then plot the average focal mechanism difference as a function of length for these two sets of simulations on top of Hardebeck's data to assess our fit. The 3D simulations have a limited spatial frequency bandwidth, a little under two orders of magnitude, for several reasons: 1) The size of our grids in 3D is limited, unless we go to a supercomputer, because the number of points increases as $N^3$. Currently, all computations are being done on an Apple G5 computer so we limit ourselves to 201x201x201 grids. 2) The periodic boundary condition on the heterogeneity means that the average focal mechanism difference reaches a maximum at approximately $10^2$ times the spacing between points, $10^2$ grid spaces. 3) Distances less than 3 grid spaces produce unstable average focal mechanism differences because at that scale the discretization of the heterogeneous grid becomes important. Therefore, in Figure 5.8 our 3D results are plotted with solid lines for a bandwidth of 3 –100 grid spaces, a little under two orders of magnitude, where each grid space would approximately match 1 km in the real Earth.

To extrapolate to smaller distances and cover a greater spatial frequency bandwidth, we quickly calculate synthetic focal mechanisms, using smoothed 1D heterogeneous stress as defined in Chapters 2 and 3. We generate 1D smoothed heterogeneous stress with the same parameters as the 3D simulations, but with a greater bandwidth. Using lines of 100,001 points, we bring the first 2,000 points to failure and calculate the average focal mechanism difference as a function of distance. This produces curves with spatial frequency bandwidths of about three orders of magnitude, 1 more order of magnitude than our 3D simulations. We had hoped for four orders of magnitude, but the noise in the curves prevents this. There are some aspects of the 1D simulations we still need to study. In Figure 5.8 we just plot one simulation for Southern California and one plot for East Bay, San Francisco to give an initial idea. The 1D simulations are drawn with dashed lines and begin where the 3D simulations leave off. The 1D simulations for distances greater than 2 km become very noisy, but still generally follow the 3D numerical simulation curves and Hardebeck's [in review, 2006] data.

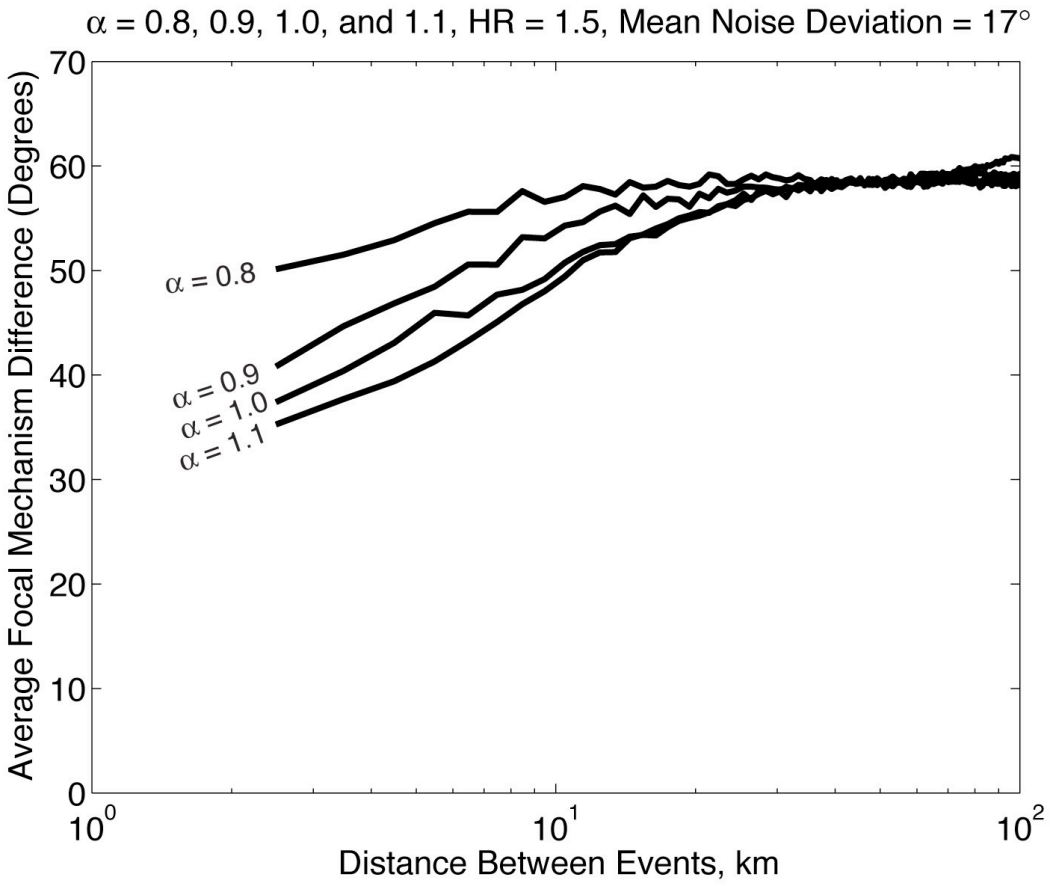


**Figure 5.5.** *Using the same random seed grid for each* $\alpha$ *, we run four different simulations for each curve and plot the average. Each curve has a heterogeneity ratio,* $HR = 1.5$ *, and an* $\omega$ *mean deviation of 17°. The spatial smoothing parameter,* $\alpha$ *, is varied, where* $\alpha = 0.8$ *corresponds to the most shallow curve on top, and* $\alpha$ *increases by 0.1 for each successive curve. As* $\alpha$ *increases, so does the slope of the average focal mechanism difference as a function of interevent distance. Interestingly,* $\alpha$ *does not appear to affect the maximum level at far interevent distances.*

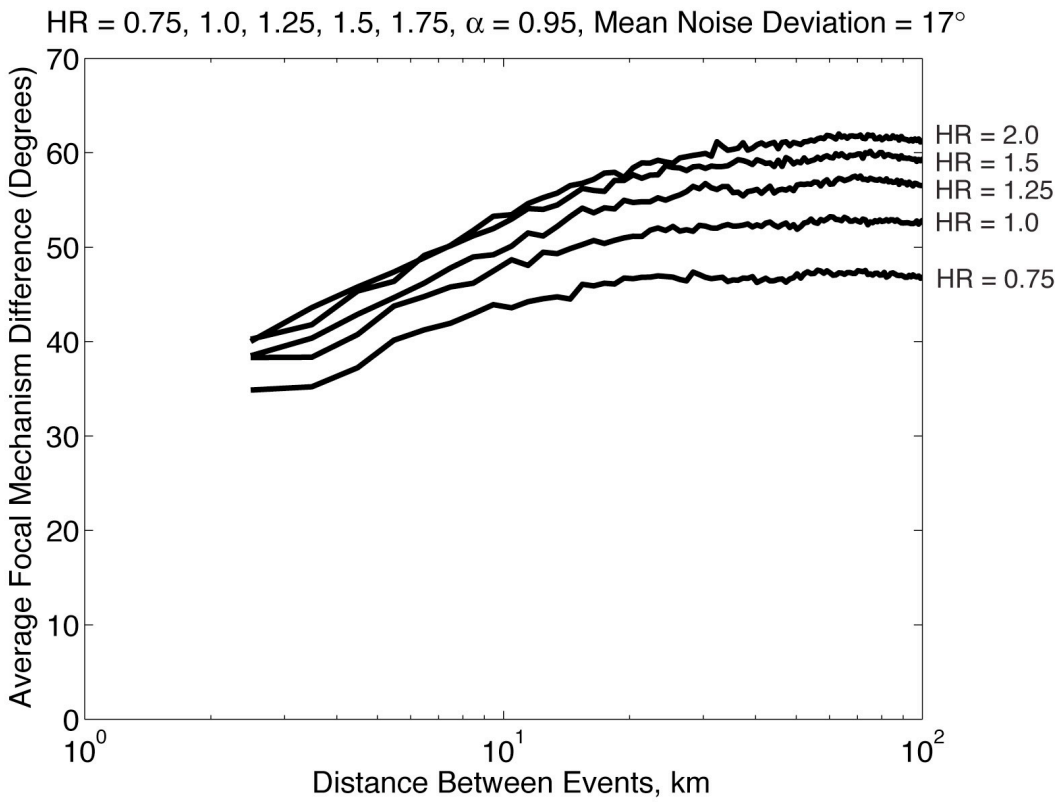


**Figure 5.6.** *Using the same random seed grid we run four different simulations for each curve and plot the average. Each curve has an* $\alpha = 0.95$ *and an* $\omega$ *mean deviation of 17°. The heterogeneity ratio,* $HR$*, is varied from* $HR = 0.75 - 2.0$*. As* $HR$ *increases, the maximum average focal mechanism difference increases. Since* $\alpha$ *does not affect the maximum average focal mechanism difference and* $HR$ *does, if we can fix the noise level, we can estimate* $HR$ *from the maxima in Hardebeck's [in review, 2006] data.*

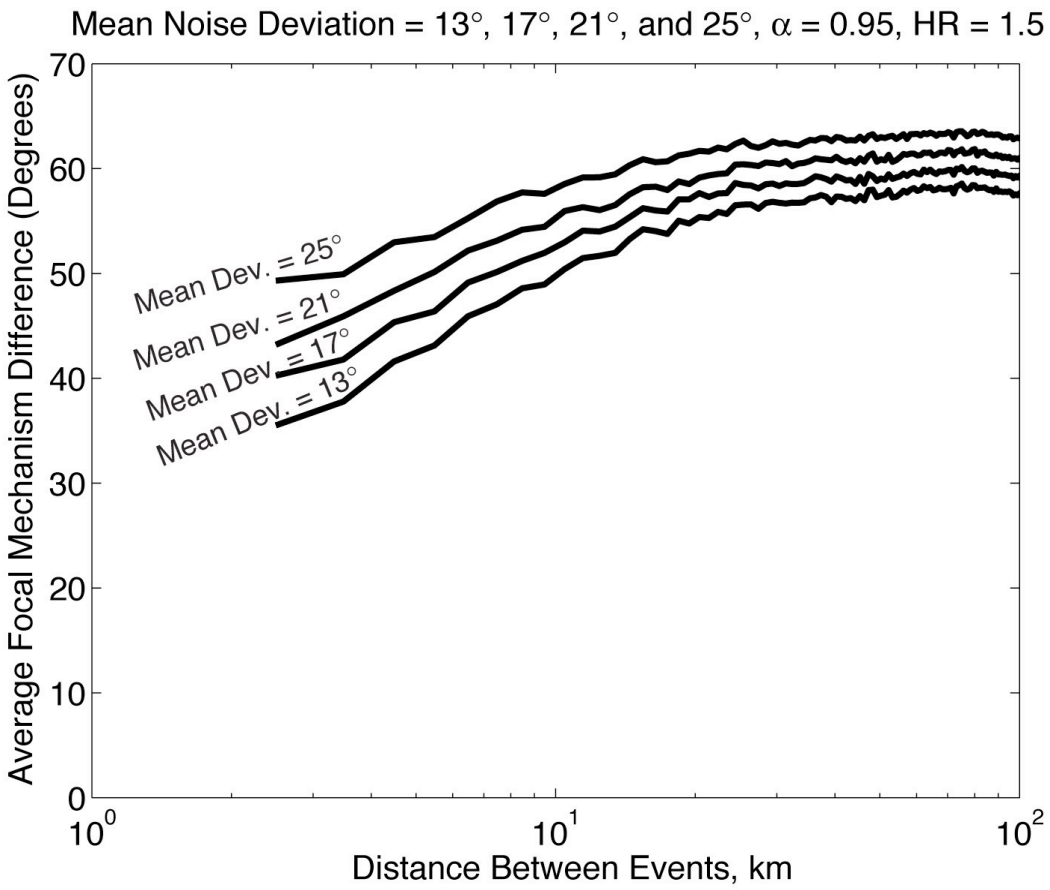


**Figure 5.7.** *Using the same random seed, we run four different simulations for each curve and plot the average. Each curve has an* $\alpha = 0.95$ *and an* $HR = 1.5$. *The* $\omega$ *mean deviation (focal mechanism uncertainty in real data) is varied from 13°–25° to show the effect of model noise on the simulations. As the mean deviation of the noise increases, two things happen. The curve's maximum increases, and the slope decreases. Therefore, it is important to have an accurate estimate of the model noise to parameterize both the heterogeneity ratio,* $HR$ *and the spatial smoothing parameter,* $\alpha$.

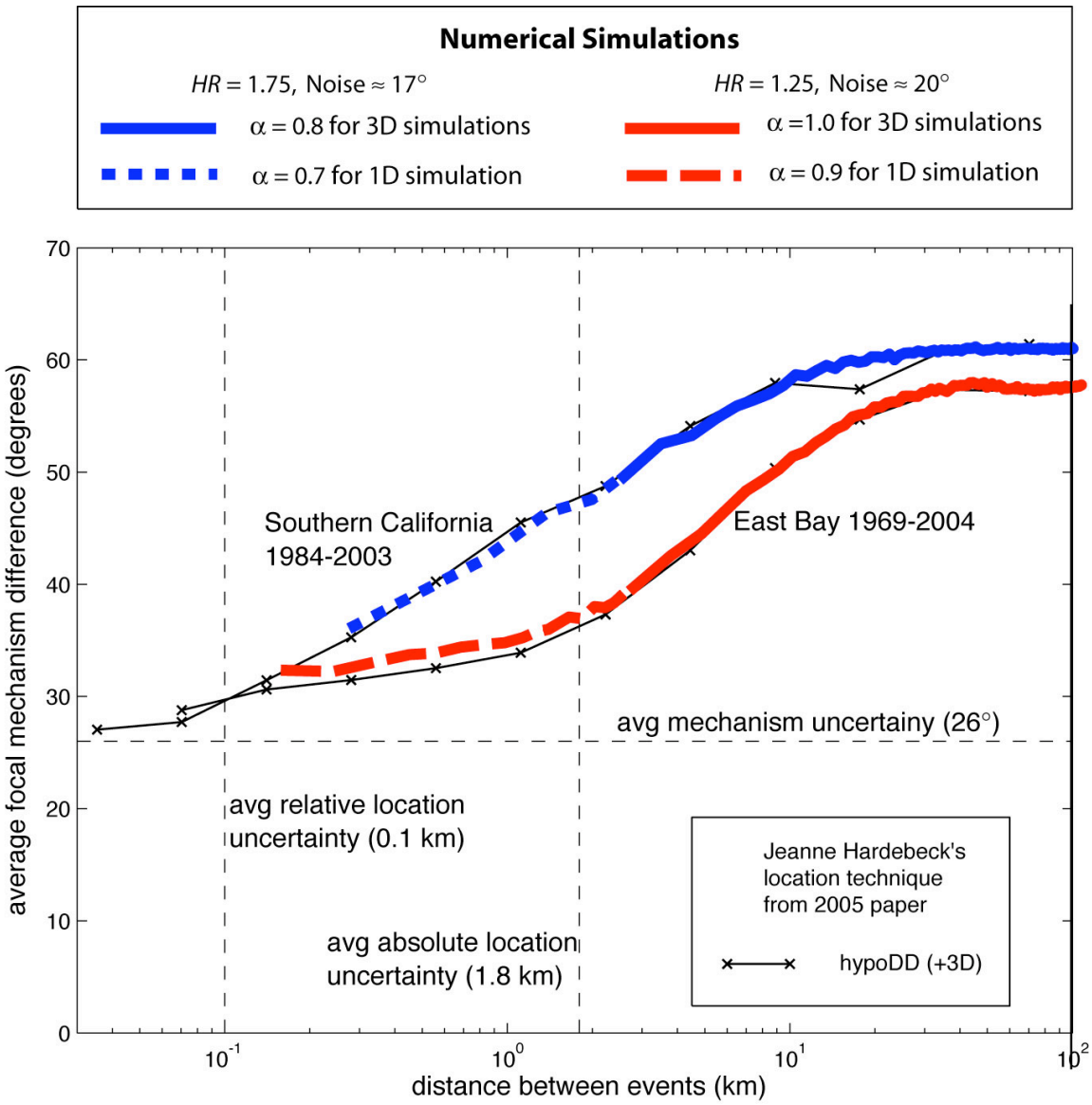


**Figure 5.8.** *Figure modified from Hardebeck [in review, 2006]. The thin black line for Southern California and East Bay is Hardebeck's HypoDD (+3D) solution for those two regions. The average focal mechanism difference increases with distance between focal mechanism pairs, indicating there is some type of smoothed heterogeneity. We calculate 3D and 1D simulations that seem to best fit the curves. We plot our results on top of Hardebeck's data, with solid lines for our 3D simulations and dashed lines for our 1D extrapolations. We find a heterogeneity ratio,* $HR = 1.75$ *, for Southern California in*

*both our 3D and 1D simulations, and an* $HR = 1.25$ *for East Bay in both our 3D and 1D simulations. The spatial smoothing parameter,* $\alpha$ *, estimated from these two types of simulations is slightly different. The value of* $\alpha$ *is approximately 0.1 lower in the 1D simulations for both Southern California and East Bay, San Francisco. Whether that is due to the reduced dimensionality or the increased bandwidth is yet to be determined. Our guess is that this is an effect of increased bandwidth in the simulation, and if we were to simulate the entire bandwidth of Hardebeck's data, almost four orders of magnitude, we might predict an* $\alpha = 0.6$ *for Southern California and an* $\alpha = 0.8$ *for East Bay, San Francisco.*

*Southern California may have a larger* $HR$ *and smaller* $\alpha$ *than East Bay, San Francisco, due to the inclusion of aftershocks from moderate earthquakes such as Northridge, Landers, and Hector Mine.*

The 3D simulations give the following heterogeneity parameter estimates for Southern California, a spatial smoothing parameter, $\alpha = 0.8$, and an $HR = 1.75$ for a model noise level of 17° mean $\omega$ deviation. The initial 1D simulation uses the same $HR = 1.75$ and mean deviation of 17°, but requires a slightly smaller spatial smoothing parameter to fit the data, an $\alpha = 0.7$. From our 3D simulations of East Bay, San Francisco, we estimate an $\alpha = 1.0$ and $HR = 1.25$ with a model noise mean deviation of 20°, and from our initial 1D simulations, we estimate an $\alpha = 0.9$ and $HR = 1.25$ with a model noise mean deviation of 20°. While the 1D simulations require the same $HR$ as the 3D simulations, the 1D simulations with the greater bandwidth require a spatially rougher stress, i.e., smaller values of $\alpha$.

If we increase the bandwidth again to produce average focal mechanism difference as a function of distance to match Hardebeck's entire plots, we might predict our estimates of $\alpha$ to be lower once again (Table 5.2). This gives us a range of $\alpha = 0.6 - 0.8$ for Southern California and $\alpha = 0.8 - 1.0$ for East Bay, San Francisco. The heterogeneity ratios would still be $HR = 1.75$ for Southern California and $HR = 1.25$, for East Bay, San Francisco. Again these values of $\alpha$ are our best guess for now. What is particularly important in our parameterization is the heterogeneity ratio, $HR$, because this determines to what degree the focal mechanism inversion results are biased toward the stress rate tensor. Fortunately, $HR$ appears to be a stable quantity in these parameterizations regardless of what $\alpha$ we use or spatial bandwidth we have.

Our guess as to why Southern California has a larger $HR$ than East Bay, San Francisco, and smaller $\alpha$, may be that Southern California includes aftershock data from moderate earthquakes such as Northridge and Landers. Initial simulations (not shown) of

aftershocks due to moderate-major earthquakes suggest that aftershocks tend to have a larger average focal mechanism difference than background seismicity because the significant static stress change accesses a greater variety of stress states, which would raise the $HR$ estimate. Also, the mainshock may roughen the local stress state immediately after the earthquake [*Ben-Zion, et al.*, 2003] resulting in a lower estimate of the parameter $\alpha$. In Figure 5.2, the curve for Southern California begins to flatten out at the same maximum angular difference as East Bay, San Francisco, about 57°, then begins to ramp up again and flattens out finally at approximately 62°. Our speculation is that the background seismicity in Southern California may actually have parameters similar to East Bay, San Francisco, an $HR = 1.25$, and predicted $\alpha = 0.8$. Adding the effects of aftershocks may produce a plot similar to Figure 5.2 for Southern California.

**Table 5.2.** Estimated Heterogeneous Parameters for Southern California and East Bay, San Francisco

| | $\alpha$ Estimate for 3D simulations | $\alpha$ Estimate for 1D simulation | $\alpha$ Predicted | HR for all simulations |
|---|---|---|---|---|
| Southern California | 0.8 | 0.7 | 0.6 | 1.75 |
| East Bay, San Francisco | 1.0 | 0.9 | 0.8 | 1.25 |

*These are the estimated parameters from Figure 5.8. Because of the limited bandwidth of the 3D simulations, we probably overestimate the spatial smoothing parameter,* $\alpha$. *The 1D simulations with greater bandwidth, almost three orders of magnitude spatially, lead us to estimates of* $\alpha$, *approximately 0.1 less than the 3D simulations. If we were to successfully model the entire bandwidth shown in Figure 5.8, it may lower the estimates of* $\alpha$ *once more. The best we can say at this point is that an* $\alpha$ *in the range of* $0.6 - 0.8$, *may fit the data for Southern California, and an* $\alpha$ *in the range of* $0.6 - 0.8$ *may fit the data for East Bay, San Francisco. Interestingly, the 1D simulations work with the same* $HR$, $HR = 1.75$ *for Southern California and* $HR = 1.25$ *for East Bay, San Francisco; therefore, this parameter may be insensitive to bandwidth*.

**Comparing Inversions of Real Focal Mechanism Data to Inversions of Our Synthetic Focal Mechanisms**

Using Hardebeck's 1984–2003 Southern California data set [*Hardebeck and Shearer*, 2003] from the web site, www.data.scec.org/research/altcatalogs.html, we apply Andy Michael's "slick" focal mechanism inversion program to A and B quality data for seven regions. We attempt to avoid aftershock zones such as Northridge, Landers, and Hector Mine. Using a type of bootstrapping for each region, we resample the region until we have 1,000 focal mechanisms, invert the data, and repeat this 50 times. We then average two of the statistics, mean misfit angle and the standard deviation of the misfit angle over the 50 inversions. See Table 5.3 and Figure 5.9 for the P-T plots of the seven regions we sample and the statistics we compute.

In order to compare our synthetic focal mechanisms to the real focal mechanisms, we apply the inversion program "slick" to our numerical simulations in the following manner. For each simulation we add model noise (to simulate focal mechanism measurement error) with a specified mean deviation, invert 1,000 noisy focal mechanisms, repeat this 50 times (adding a different random noise each time), and average the mean misfit angle and standard deviation misfit angle over the 50 sets. We create these statistics for $\alpha = 0.0, 0.5, \text{and } 1.0$, $HR = 0.1 - 100$, and mean $\omega$ deviation = 17°, 20°, and 26°, to examine the effect of each parameter. Typically, the greater the heterogeneity is, $HR$, the larger the mean misfit angle and the standard deviation of the misfit angle. Varying $\alpha$, for $\alpha = 0.0 - 1.0$, appears to have little to no effect on the statistics. Increasing the noise, the mean $\omega$ deviation also increases the mean misfit angle and the standard deviation of the misfit angle.

**Table 5.3.** Seven Study Regions in Southern California from A and B Quality Focal Mechanism Data

| | Latitude Range (°N) | Longitude Range (°E) | Mean Misfit Angle (Degrees) | Standard Deviation of the Misfit Angle (Degrees) | Number of Points |
|---|---|---|---|---|---|
| Test Region 1 LA Basin | 33.75–34.25 | 241.2–241.7 | 18.0641 | 20.7630 | 192 |
| Test Region 2 San Gabriel Mountains | 34.25–34.5<br>34.4–34.7<br>34.5–37.5 | 241.75–242.25<br>241.5–241.75<br>241.25–241.5 | 24.7288 | 25.7336 | 64 |
| Test Region 3 | 33.5–33.75 | 243–243.25 | 24.2155 | 25.7085 | 170 |
| Test Region 4 | 33.75–34 | 243–243.25 | 23.6730 | 20.1619 | 260 |
| Test Region 5 | 33.5–33.75 | 243.25–243.5 | 25.9741 | 21.6666 | 215 |
| Test Region 6 | 33.25–33.5 | 243.5–243.75 | 22.3788 | 22.2544 | 191 |
| Test Region 7 | 33.75–34 | 243.5–243.75 | 21.1410 | 19.6019 | 222 |

*We picked seven regions to study, preferably with minimal aftershock activity. Columns 2 and 3 are the Latitudes and Longitudes that prescribe the box within which we choose focal mechanisms for the seven regions from the A and B quality data [Hardebeck and Shearer, 2003]. Using a type of bootstrapping explained in the text, we calculate the mean misfit angle and the standard deviation of the misfit angle for our three regions. These values are plotted in Figures 5.10–5.12. Then in Figure 5.13 we use the mean misfit values for each region to estimate their heterogeneity ratios, HR.*

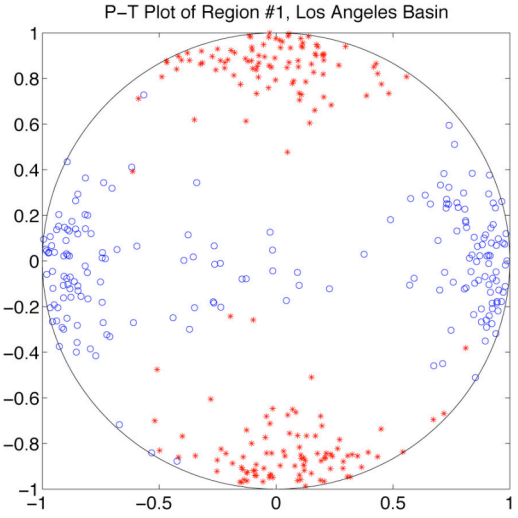
P–T Plot of Region #1, Los Angeles Basin

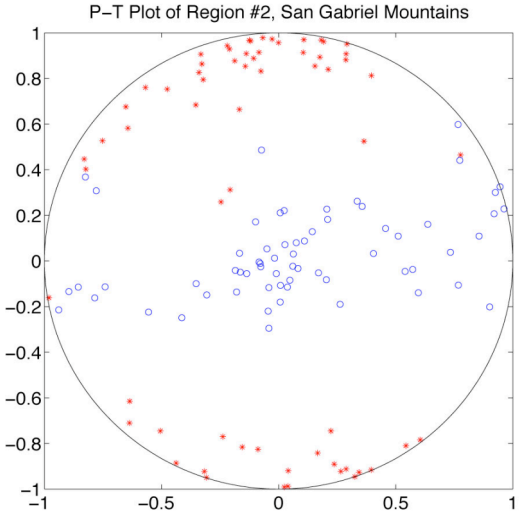
P–T Plot of Region #2, San Gabriel Mountains

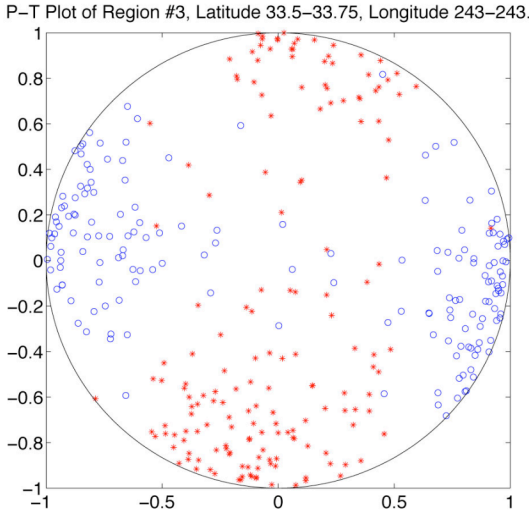
P–T Plot of Region #3, Latitude 33.5–33.75, Longitude 243–243.25

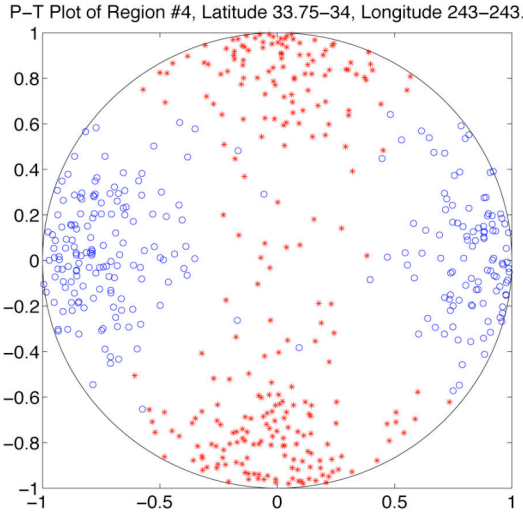
P–T Plot of Region #4, Latitude 33.75–34, Longitude 243–243.25

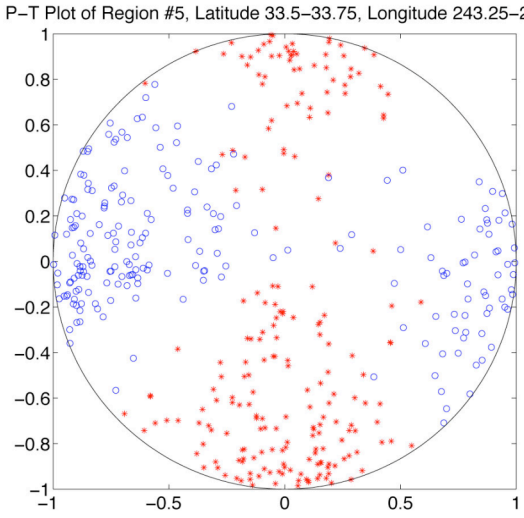
P–T Plot of Region #5, Latitude 33.5–33.75, Longitude 243.25–243.5

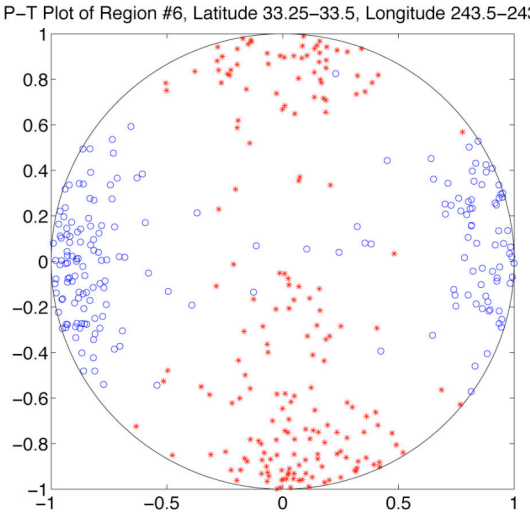
P–T Plot of Region #6, Latitude 33.25–33.5, Longitude 243.5–243.75

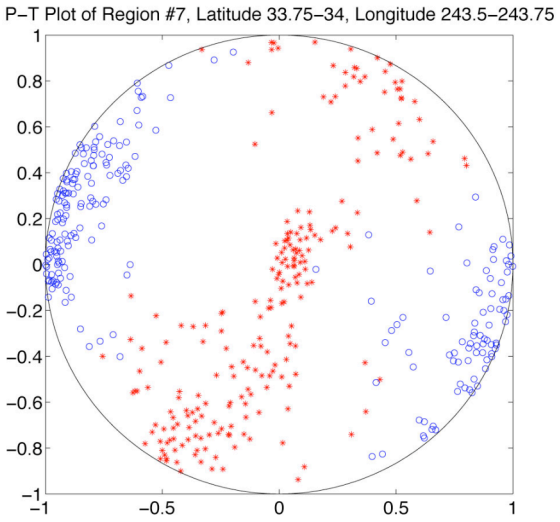


**Figure 5.9.** *P-T plots of the seven study regions from the A and B quality focal mechanism data. The red asterisks represent the P (compression) axes and the blue open circles represent the T (tension) axes for each focal mechanism.*

Interestingly, measurement noise and heterogeneity appear to increase these two statistics differently. Defining a new parameter, which we will call the misfit ratio,

$$MR = \frac{\text{Mean Misfit Angle}}{\text{Standard Deviation of the Misfit Angle}}, \tag{5.5}$$

we find that if there is only model noise and no stress heterogeneity one would expect a $MR \approx 0.7$. If there is no model noise and only stress heterogeneity, one could achieve a $MR \approx 1.5$. One way of assessing whether or not a mean deviation of 17° is appropriate for Southern California is to compare the mean misfit angle and the standard deviation of the misfit angle for our simulations with different $\alpha$, $HR$, and noise to our seven regions in Table 5.3. In Figures 5.10, we explore this by plotting mean misfit angle vs. standard deviation of the misfit angle for our simulations and for our seven regions of real focal mechanism data. Generally, as $HR$ increases (variable not shown), both the mean misfit

angle and the standard deviation of the misfit angle increase, creating the lines seen in Figure 5.10. The three red dashed lines represent $\alpha$ = 0.0, 0.5, and 1.0 , for the simulation background stress, "Southern San Andreas," $\boldsymbol{\sigma}'_{B_2}$ , from Chapter 4 with a mean model noise deviation of 17° added to the synthetic focal mechanisms. The three solid blue lines represent $\alpha$ = 0.0, 0.5, and 1.0 , for the simulation background stress, "San Gabriel Mountains," $\boldsymbol{\sigma}'_{B_1}$ , from Chapter 4, with a mean model noise deviation of 17° added to the synthetic focal mechanisms. The lines follow the path of increasing heterogeneity, $HR$ , in the mean misfit angle vs. standard deviation of the misfit angle space. We plot small solid circles for the end-member, $HR = 0$ , case from Table 5.1. Last, we plot the values computed for our seven regions listed in Table 5.3, with black asterisks. The point of this graph is to show that the real data, with black asterisks, are compatible with the predicted mean misfit angles and standard deviation of the misfit angles from our numerical simulations when we add a mean model noise deviation of 17° to our synthetic focal mechanisms. The real data points fall within the possible range of values. In Figure 5.11, we have the exact same graph but now a mean model noise deviation of 20° has been added to our synthetic focal mechanisms and our synthetic lines are no longer centered on the real data, indicating 20° could be an overestimate for Southern California data, at least for these seven regions. Increasing the mean model noise deviation again to 26°, we plot in Figure 5.12 the same information. The real data are completely offset from our synthetic curves, indicating that a mean noise deviation of 26° is an overestimate of noise for those regions in Southern California. These results give us increased confidence in using our mean model noise deviation of 17° when parameterizing $\alpha$ and $HR$ in Southern California.

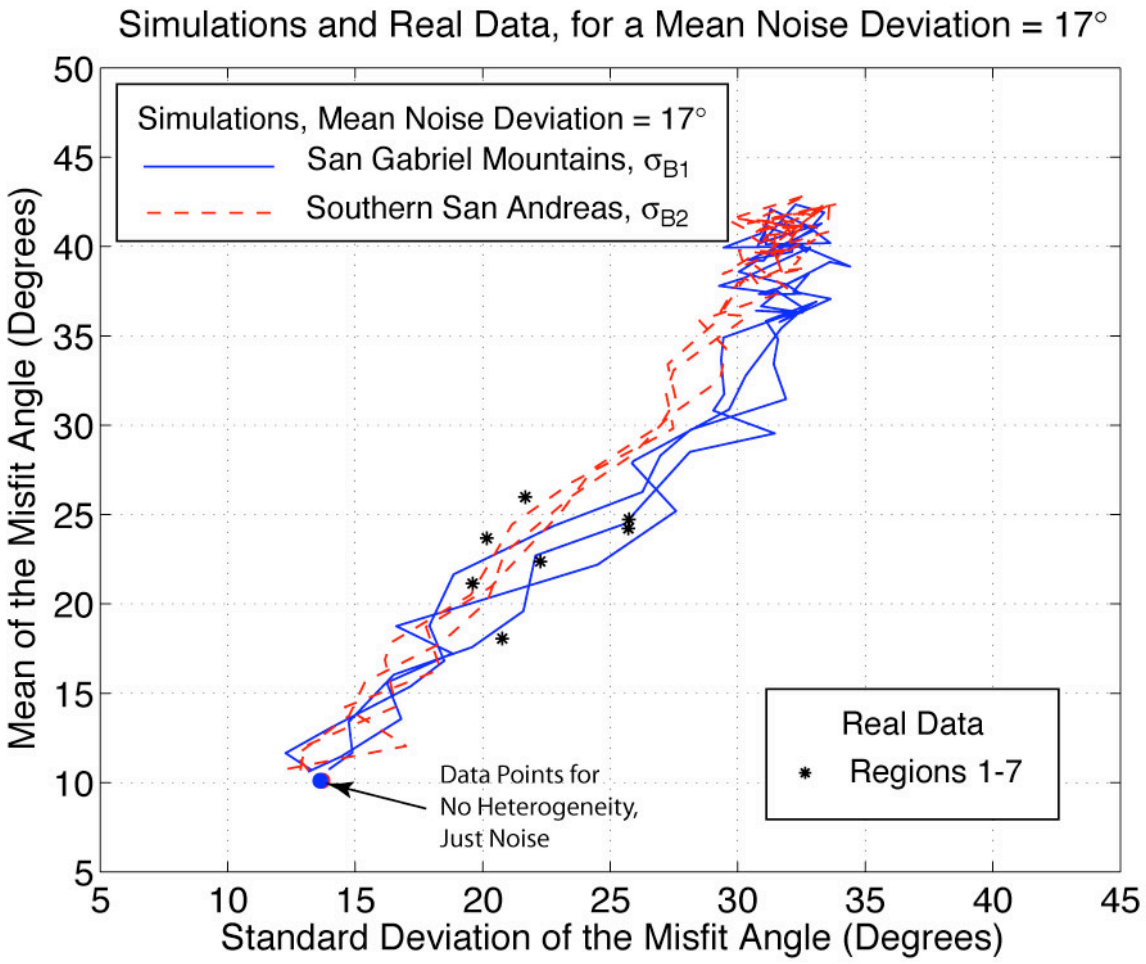


**Figure 5.10.** *In this Figure we compare two observables, mean misfit angle and the standard deviation of the misfit angle, for noisy simulated focal mechanisms and real data from our regions 1–7. While these two parameters should be linearly related for a Gaussian distribution, the distributions of focal mechanism orientations are not necessarily Gaussian. When we start adding model noise to our synthetic, heterogeneous focal mechanisms, we find that the ratio of mean misfit angle vs. standard deviation of the misfit angle, MR, depends on how much of the scatter comes from model noise vs. true stress heterogeneity. In this plot, we add noise with a mean model noise deviation*

*of 17° (what we use when trying to parameterize Southern California in Figure 5.8) to our synthetic focal mechanisms, invert the focal mechanisms to calculate the mean misfit angle and standard deviation of the misfit angle, repeat this procedure fifty times, and average the two parameters. We do this for a range of* $HR = 0.1 - 100$ *and plot the path of increasing* $HR$ *in the mean misfit angle vs. standard deviation of the misfit angle space. The red dashed lines are for* $\alpha = 0.0, 0.5,$ and $1.0$*, using the "Southern San Andreas" background stress,* $\boldsymbol{\sigma}'_{B_2}$*, from Chapter 4. The blue solid lines are for* $\alpha = 0.0, 0.5,$ and $1.0$ *using the "San Gabriel Mountains" background stress,* $\boldsymbol{\sigma}'_{B_1}$*, from Chapter 4. We find that the* $\alpha$ *parameter has little to no effect on the calculation of the mean misfit angle or standard deviation of the misfit angle parameters. The black asterisks are the seven study regions. We find that their mean misfit angle and standard deviation of the misfit angle fall within the possible values for our noisy simulated data. The real data for seven regions in Southern California are nicely centered on the simulated curves. Therefore, it appears that the addition of a mean model noise deviation of 17° to our synthetic focal mechanisms produces statistics compatible with real data.*

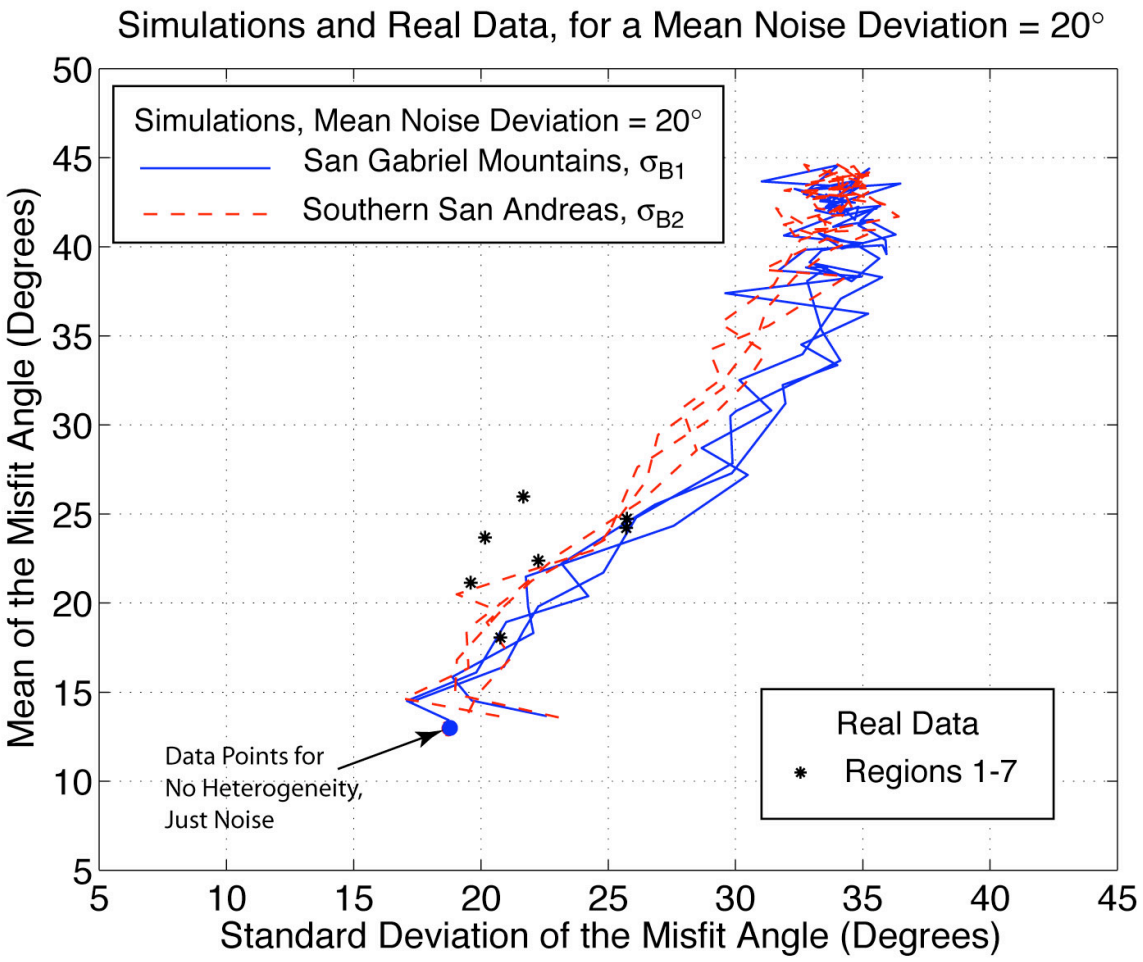


**Figure 5.11.** *Symbology as in Figure 5.10, with a mean model noise deviation of 20° added to the synthetic focal mechanisms. The paths of increasing heterogeneity in the mean misfit angle vs. standard deviation of the misfit angle space no longer center on the real data in black asterisks, our Southern California regions 1–7. Instead, the paths are slightly offset to the bottom right. This level of model noise is what we use for the East Bay San Francisco parameterization, but it appears that it is not as compatible as 17° for the Southern California data. This is a good check. It shows that we most likely use the correct level of model noise, mean deviation of 17°, for our parameterization of Southern California.*

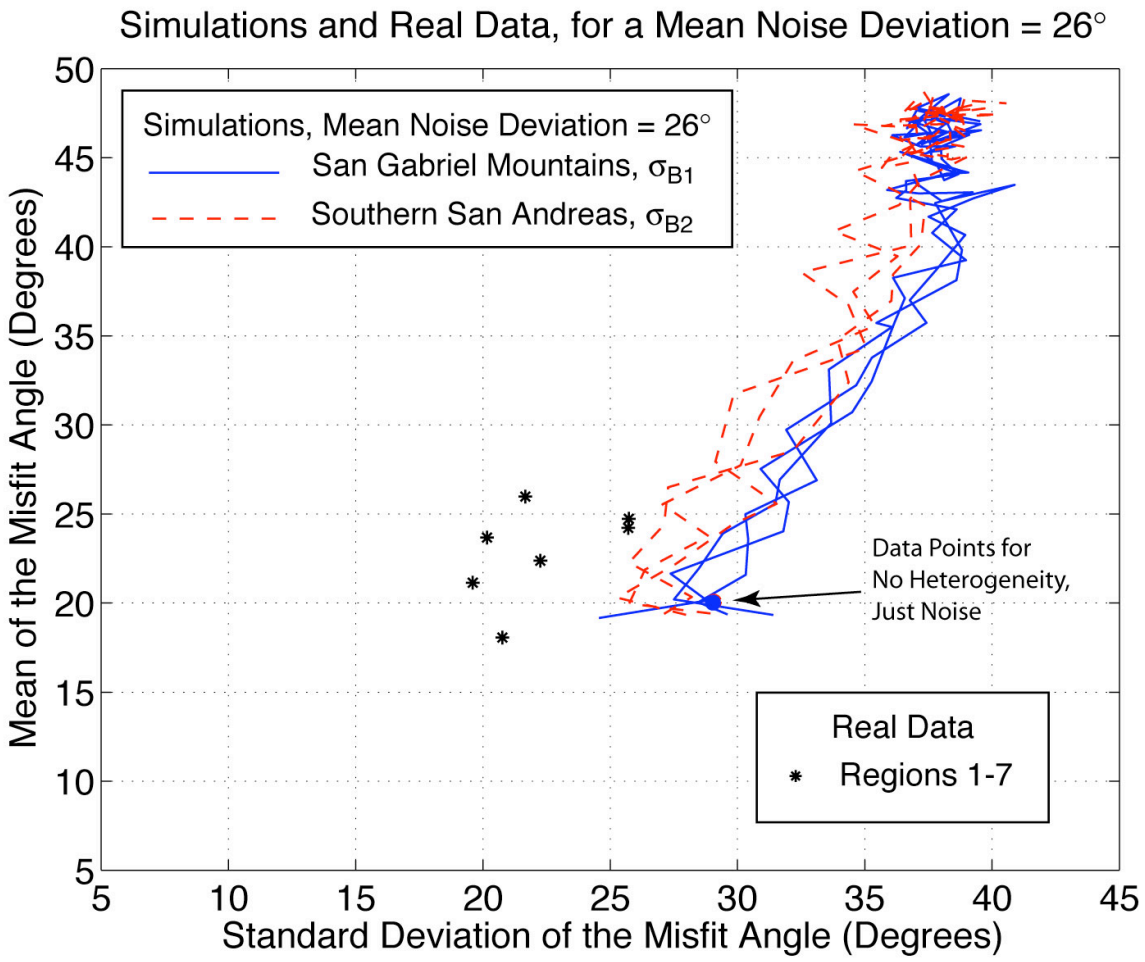


**Figure 5.12.** *Same type of plot as Figures 5.10 and 5.11, only we further increase the mean model noise deviation to 26°. In this case, the paths of increasing heterogeneity, the red dashed and blue solid lines, for our noisy simulated data are completely offset from the real Southern California data. This indicates that a mean deviation of 26° overestimates the model noise for background seismicity in Southern California.*

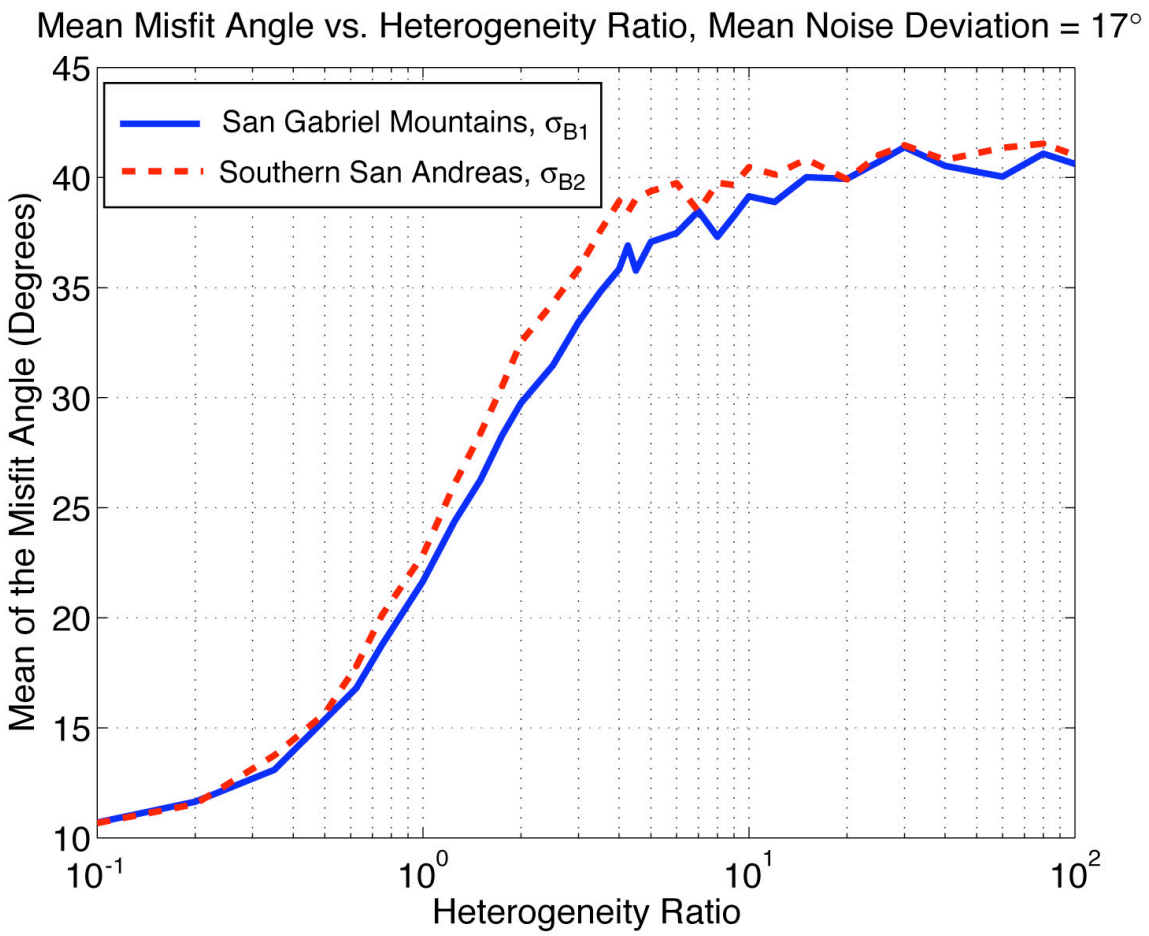


**Figure 5.13.** *This plot of mean misfit angle as a function of Heterogeneity Ratio, HR was constructed by adding a mean model noise deviation of 17° to our synthetic focal mechanisms for* $\alpha = 1.0$, *inverting the focal mechanisms using the program "slick" [Michael, 1984; 1987] to produce the mean misfit angle, repeating this 50 times, then averaging the mean misfit angle. The solid blue line uses the simulations with the "San Gabriel Mountains" background stress,* $\sigma'_{B_1}$, *and the dashed red line uses the simulations with the "Southern San Andreas" background stress,* $\sigma'_{B_2}$, *both introduced in Chapter 4. For these two very different background stresses, the mean misfit angle vs. HR curves are fairly similar. Of greater interest is that the increase of mean misfit angle as a function of HR has a very similar shape to the curves in Figure 4.12. In*

*Figure 4.12, we plot the percent bias toward the stress rate tensor, $\dot{\boldsymbol{\sigma}}'_T$, as a function of $HR$. This gives us hope that there may be a linear relationship between mean misfit angle for real data and the bias toward the stress rate tensor, $\dot{\boldsymbol{\sigma}}'_T$.*

It is true that the mean misfit angle and the standard deviation of the misfit angle are related by a constant for a 1D Gaussian distribution; therefore, in our attempt to vary the noise until we have an appropriate misfit ratios, $MR$, that matches real data, we are really varying the shape of the distribution of the focal mechanism scatter until it is similar to what is seen in the real Earth.

Now that we have confirmed that a mean model noise deviation of ≈17° is appropriate for the Southern California, we plot in Figure 5.13 the mean misfit angle as a function of heterogeneity ratio, $HR$ for our simulated data with 17° model noise added. Presumably, we can use this relationship between mean misfit angle and heterogeneity to estimate the $HR$ for real data. In Figure 5.13, we use a mean model noise deviation of 17° added to our synthetic focal mechanisms, and we use an $\alpha = 1.0$, which is close to our estimated $\alpha$. The value of $\alpha$ has little to no effect on the curves in Figure 5.13 so it probably does not matter exactly what value to use in these calculations so long as it is close to our estimate. The solid blue line shows our results for simulations with a "San Gabriel Mountains" background stress, $\boldsymbol{\sigma}'_{B_1}$, and the red dashed lines shows our results for simulations with a "Southern San Andreas" background stress, $\boldsymbol{\sigma}'_{B_2}$. There are three features to note: 1) Mean misfit angle increases with heterogeneity ratio, $HR$. 2) The

two very different sets of simulations give similar curves. 3) The relation between mean misfit angle and $HR$ looks very similar to the relation between the normalized bias toward our stress rate tensor, $\dot{\boldsymbol{\sigma}}'_T$, and $HR$ as seen in Figure 4.12 in the previous chapter. This gives us hope that we can use the mean misfit angle in focal mechanism inversions for the real Earth to estimate both the heterogeneity ratio, $HR$, and the percent bias toward the stress rate tensor, $\dot{\boldsymbol{\sigma}}'_T$. Figure 5.14 explores this relationship, by plotting the percent bias toward $\dot{\boldsymbol{\sigma}}'_T$ from Figure 4.12 as function of mean misfit angle using the parameter, $HR$, to connect the two quantities; therefore, the solid lines are paths of increasing heterogeneity, $HR$. We plot this for our two sets of simulations, "San Gabriel Mountains," $\boldsymbol{\sigma}'_{B_1}$, and the "Southern San Andreas," $\boldsymbol{\sigma}'_{B_2}$. We find that the relationship between percent bias toward $\dot{\boldsymbol{\sigma}}'_T$ as a function of mean misfit angle is approximately a linear relationship for a mean misfit angle range of 15°–37°. The two sets of simulations produce slightly different slopes and intercepts for the linear best fits (see dashed lines in Figure 5.14), but there is some similarity. This type of relationship between percent bias and mean misfit angle needs to be studied further, and the effects of all the simulation parameters carefully dissected before we will have much confidence. At the same time, it is a starting point.

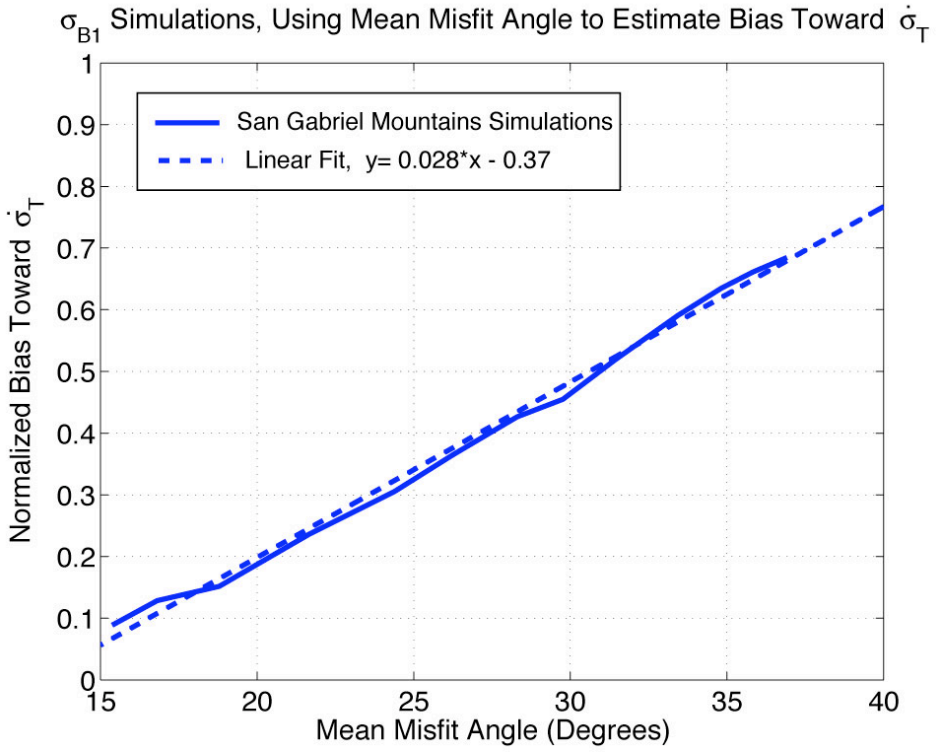


**Figure 5.14 a)**

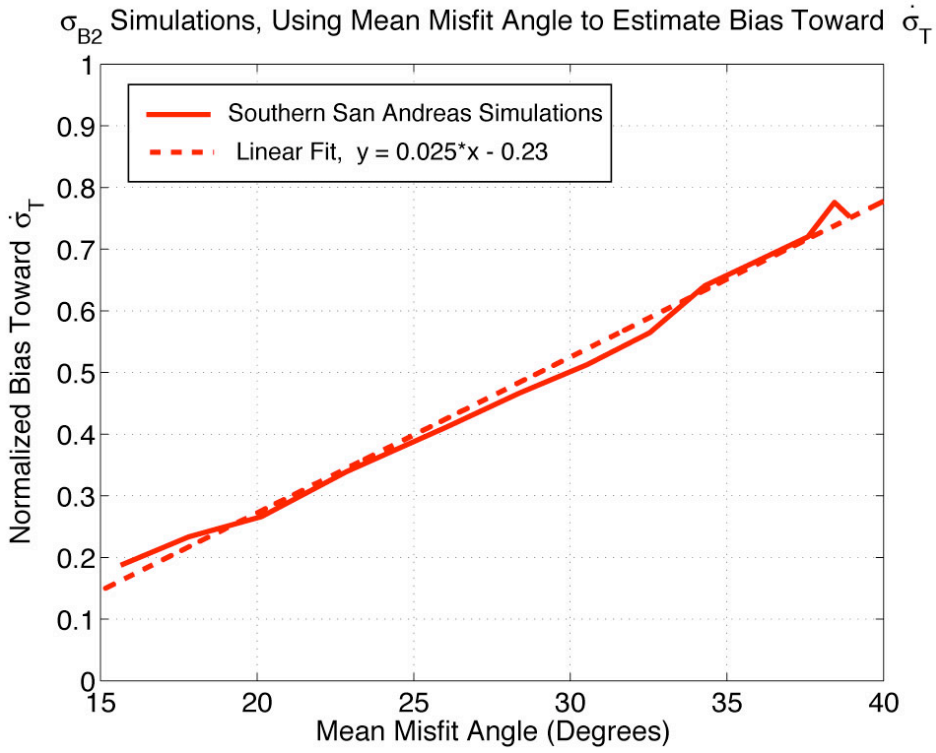


**Figure 5.14 b)**

**Figure 5.14.** *We plot paths of increasing HR in the bias toward* $\dot{\sigma}'_T$ *vs. mean misfit angle space. We use the relationship between bias and HR, and the relationship between mean misfit angle and HR to create these plots. The solid lines are our numerical simulations, synthetic focal mechanisms with* $\alpha = 1.0$*, a mean model noise deviation of 17°, averaged over 50 sets of noise. The dashed lines are the best fit linear relationships. In* ***a)*** *we plot the relationship between normalized bias and mean misfit angle for our "San Gabriel Mountains" simulations and in* ***b)*** *we plot the same relationship for our "Southern San Andreas Fault" simulations (See Chapter 4). Both sets of simulations produce a fairly linear relationship between normalized bias and mean misfit angle for a mean misfit angle range of ≈ 15–37°. The slopes and intercepts and the two lines are slightly different, but they lead to similar estimates of bias. We apply these curves to our seven regions of real focal mechanism data to estimate percent bias toward* $\dot{\sigma}'_T$ *and show the results in Table 5.4.*

Hypothetically, using this type of plot, one can subtract out the bias toward the stress rate tensor, $\dot{\boldsymbol{\sigma}}'_T$, to give the actual orientation of the background stress, $\boldsymbol{\sigma}'_B$. The procedure may be as follows:

- Select a region to study.
- Remove the aftershocks, if any, and invert the focal mechanisms within the region.
- From the mean misfit angle, estimate the heterogeneity ratio, $HR$, in the region and the percent bias toward the stress-rate tensor, $\dot{\boldsymbol{\sigma}}'_T$.
- Compare the orientation of the best-fit stress tensor from the focal mechanism inversion to the predicted stress-rate tensor from GPS data/modeling. Models like those of Becker et al. [2005] , which combine fault block modeling with GPS data as constraints, can provide the stress-rate tensors.
- If the focal mechanism inversion tensor and the stress-rate tensors are nearly identical, and $HR < 5.0$ (maximum bias of 70%), then one can estimate that the stress rate tensor, $\dot{\boldsymbol{\sigma}}'_T$, and the background stress, $\boldsymbol{\sigma}'_B$, are approximately aligned with one another.
- If there is a significant difference between the focal mechanism inversion tensor and the stress-rate tensor, and $HR > 0.5$ (minimum bias of 10%), then there is an even greater difference between the $\boldsymbol{\sigma}'_B$ and $\dot{\boldsymbol{\sigma}}'_T$. Use the estimate of the percent bias toward $\dot{\boldsymbol{\sigma}}'_T$, combined with the values of the inverted tensor, $\boldsymbol{\sigma}'_{Inverted}$, and $\dot{\boldsymbol{\sigma}}'_T$, to estimate $\boldsymbol{\sigma}'_B$.

In summary, this new methodology may enable seismologists to still use standard focal mechanism inversions to estimate $\boldsymbol{\sigma}'_B$, with the caveat that the interpretation is now

more complicated because any bias toward $\dot{\boldsymbol{\sigma}}'_T$ due to spatial stress heterogeneity needs to be removed. At the same time, this new methodology allows the estimation of a new parameter, $HR$, the ratio of the magnitudes of the spatially heterogeneous stress and the spatial mean stress, for the region. Then, using plots like Figure 5.8 to determine the spatial smoothness of the heterogeneity, $\alpha$, setting the maximum sustainable stress ≈ 200 MPa, at distance of 10 cm (what one would expect for dislocations), one may be able to estimate the size of $\boldsymbol{\sigma}'_B$ for the study region, the effective strength of the crust for the study region size [*Heaton*, 2006, in preparation].

Returning to our seven regions of real focal mechanism data, we use Figures 5.13 and 5.14 to estimate $HR$ and the percent bias toward $\dot{\boldsymbol{\sigma}}'_T$. Table 5.4 lists our estimates based on these curves. We obtain $HR$ estimates ranging from 0.62–0.70 for the LA Basin, the least heterogeneous of our seven regions, to an $HR$ = 1.21–1.44 for Region 5. We also obtain bias estimates anywhere from 14–42% bias toward the stress rate tensor, $\dot{\boldsymbol{\sigma}}'_T$; this indicates that the heterogeneity in Southern California is sufficient to significantly bias the focal mechanism inversions toward $\dot{\boldsymbol{\sigma}}'_T$, but not completely. Hypothetically, it should be possible to remove this bias due to spatially heterogeneous stress and extract the actual $\boldsymbol{\sigma}'_B$.

Interestingly, it appears that the seven regions we chose in Southern California are more compatible with an $HR = 1.25$ than the $HR = 1.75$ that we had calculated from Figure 5.8. As mentioned previously, the average focal mechanism difference as a function of distance for Southern California (Figure 5.8) includes both background seismicity and aftershocks, and we hypothesize that the inclusion of aftershocks raises the $HR$ estimate and lowers the $\alpha$ estimate. Indeed, the curve for Southern California

begins to flatten out at the same level as East Bay San Francisco, $HR = 1.25$, then begins to rise again and finally levels out at a $HR = 1.75$. Combining this information with the $HR$ estimates from comparing mean misfit angle information between our simulations and real data leads us to an estimate of $HR \approx 1.25$ and $\alpha \approx 0.8$ for regions with background seismicity (no aftershocks) in Southern California and East Bay, San Francisco.

Figure 5.15 shows P-T plots of simulation focal mechanisms using our best guess parameters and our model noise with mean deviation = 17°. We show one plot from our "San Gabriel Mountains" simulations with $\sigma_{B_1}$ and one plot from our "Southern San Andreas Fault" simulations with $\sigma_{B_2}$. The plot from our "Southern San Andreas Fault" simulations looks similar to some of the P-T plots of real data in Figure 5.9.

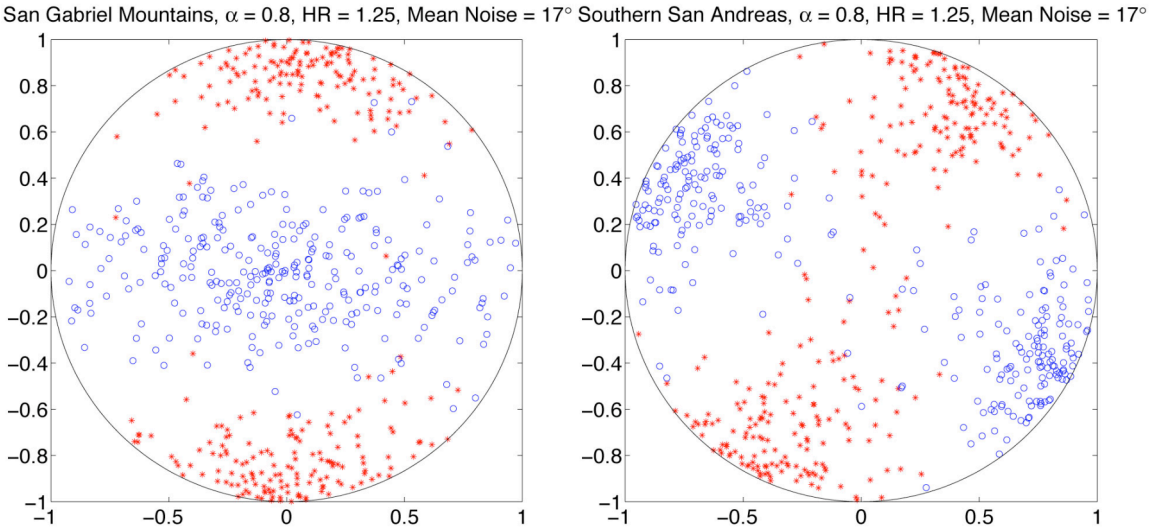


**Figure 5.15.** *P and T axes plotted for 300 synthetic focal mechanisms each, using our best guess stress heterogeneity parameters. We use an* $\alpha = 0.8$, $HR = 1.25$, *and a model noise with mean deviation = 17°. The strike-slip example on the right looks similar to some of the P-T plots of real focal mechanisms in Figure 5.9.*

In Figure 5.16 we plot what the spatial variation might look for a 1D cross section for 1 component of the deviatoric stress tensor, using our best guess parameters. We create 1D heterogeneous stress with 100,001 points and an $\alpha = 0.8$; we then add the following background stress tensor,

$$\boldsymbol{\sigma}'_B = \begin{pmatrix} 0 & 1 & 0 \\ 1 & 0 & 0 \\ 0 & 0 & 0 \end{pmatrix},$$

normalizing this background stress and our heterogeneity so that we have an $HR = 1.25$. We equate 1 grid spacing to 10 cm; therefore, our entire spatial bandwidth is approximately 10 km, or 5 orders of magnitude. We set the maximum stress at 200 MPa, which is what one may expect for granitic rock [*Scholz*, 1990], focus on a stress asperity, and calculate what the mean stress may be on a variety of length scales. This is motivated by a hypothesis from Heaton that strength in the Earth is length scale dependent [*Heaton*, 2006, in preparation]; if so, averagering stress over different length scales produces different estimates of strength. Interestingly, if we average over different length scales around the asperity, we calculate for one of the components of the deviatoric stress tensor, $\sigma_{12}$:

- ≈ 54 MPa if we average over 10 km
- ≈ 72 MPa if we average over 1 km, centered on the asperity
- ≈ 111 MPa if we average over 100 m, centered on the asperity
- ≈ 150 MPa if we average over 10 m, centered on the asperity

The increase of mean stress as we narrow our focus on the stress asperity, i.e., reduce the window over which we average, supports Heaton's hypothesis that strength in the crust depends on the length scale of the measurement.

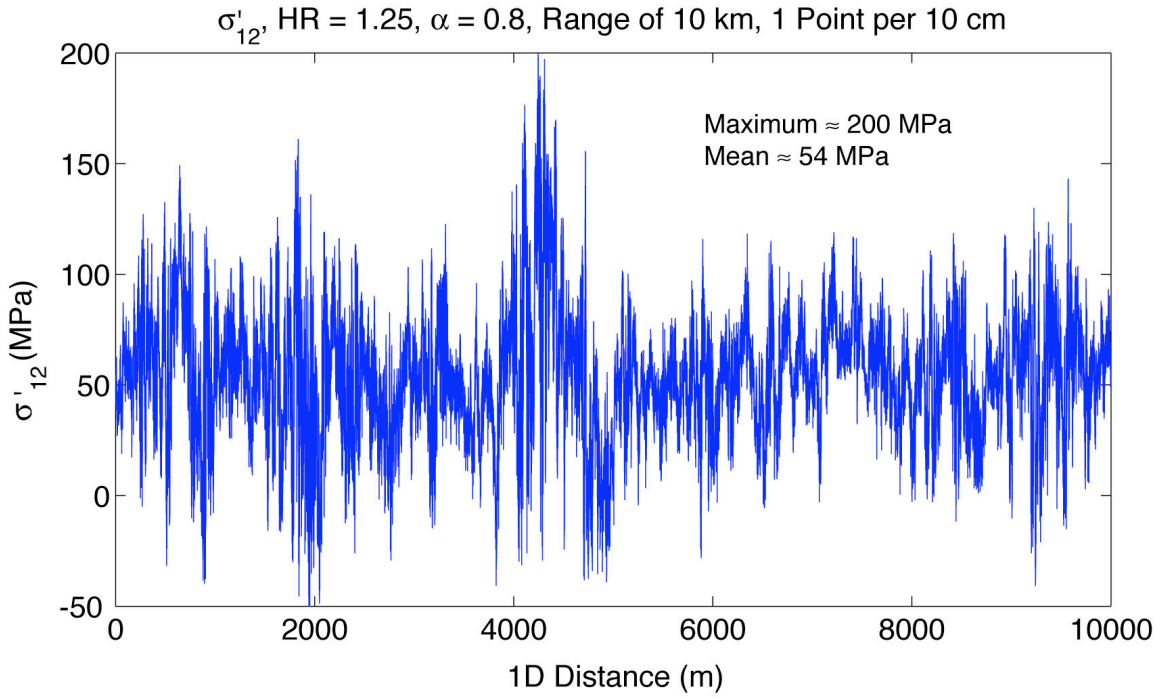


**Figure 5.16 a)**

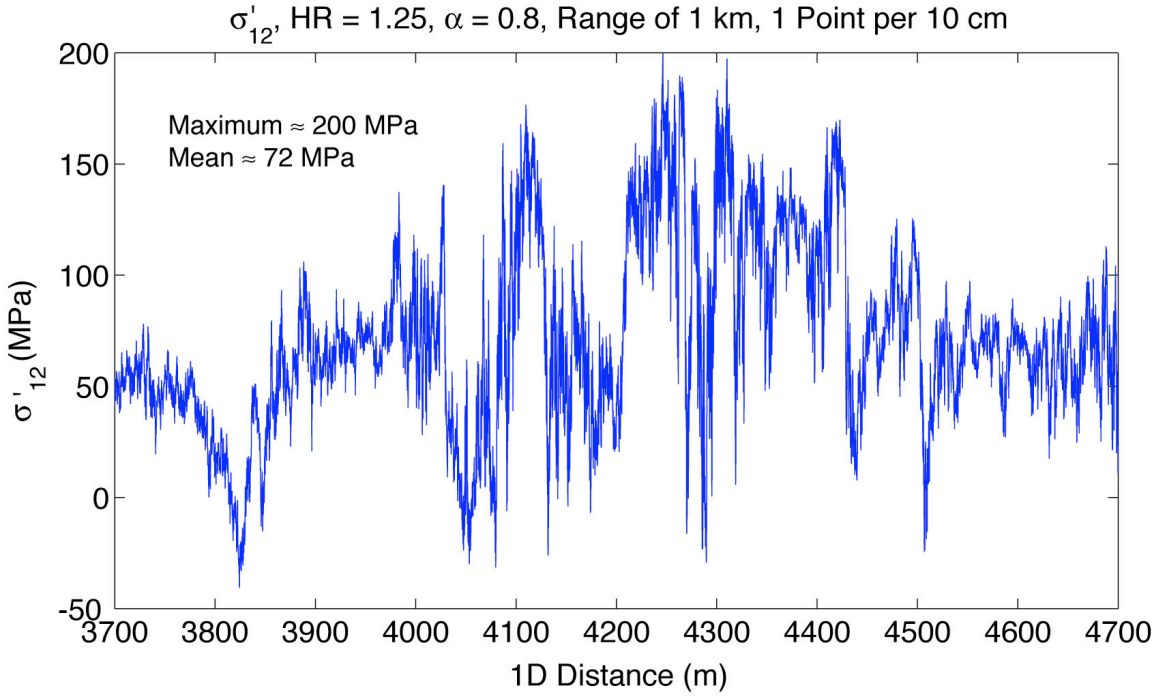


**Figure 5.16 b)**

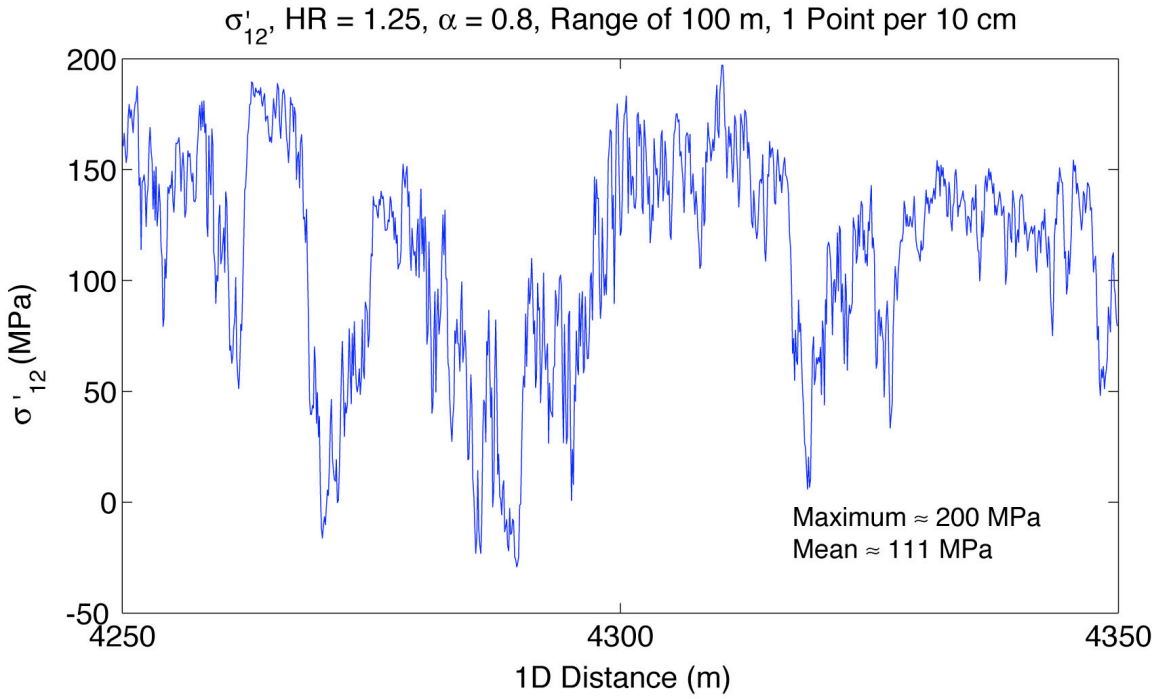


**Figure 5.16 c)**

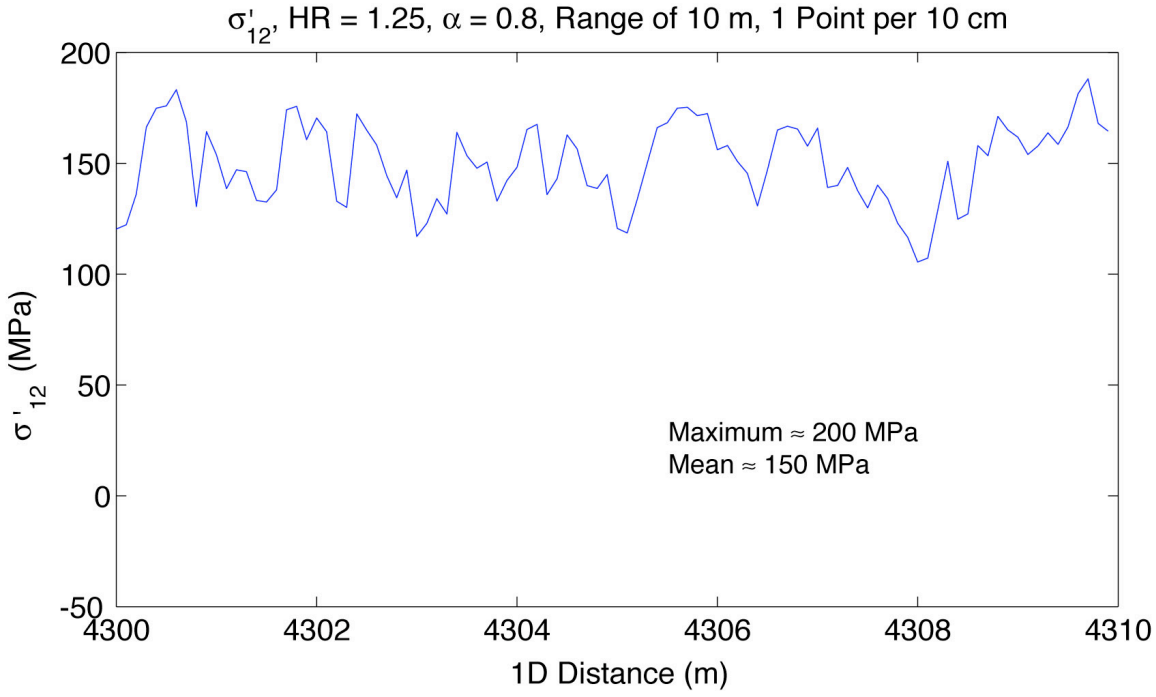


**Figure 5.16 d)**

**Figure 5.16.** *We create spatially smoothed heterogeneous stress in 1D with* $\alpha = 0.8$ *and add a spatially uniform background stress with an* $HR = 1.25$. *Therefore, it has the parameters we hypothesize for heterogeneous stress in East Bay, San Francisco and for Southern California if one were to subtract out aftershocks. We plot 100,001 points of one component of the stress tensor,* $\sigma'_{12}$ *in* ***a)***. *If we let the grid spacing equal 10 cm, then the entire range of our stress 1D cross section is approximately 10 km. In* ***a)*** *we plot the entire width, a 10 km length. In* ***b)***, ***c)***, *and* ***d)*** *we successively narrow our plotting window by an order of magnitude each time, to focus in on a stress asperity. If we set our maximum stress to be 200 MPa, what one might expect for a 10 cm dislocation, then we can estimate mean stresses at different length scales for the asperity. The mean stress tends to increase as the window narrows over which we average the stress, supporting Heaton's hypothesis [2006, in preparation] that the strength of the crust is length scale dependent.*

**Table 5.4.** Estimates of the Heterogeneity Ratio, $HR$, and the Percent Bias Toward the Stress Rate Tensor for Our Seven Regions of Real Focal Mechanism Data

| | Mean Misfit Angle | Estimate of Heterogeneity Ratio, *HR* | Estimate of Tensor Dot Tensor Dot Product Bias Toward $\dot{\boldsymbol{\sigma}}_T$ |
|---|---|---|---|
| Test Region 1 LA Basin | 18.0641 | 0.62–0.70 | 14–28% |
| Test Region 2 San Gabriel Mountains | 24.7288 | 1.14–1.31 | 32–39% |
| Test Region 3 | 24.2155 | 1.09–1.24 | 31–38% |
| Test Region 4 | 23.6730 | 1.06–1.18 | 29–36% |
| Test Region 5 | 25.9741 | 1.21–1.44 | 36–42% |
| Test Region 6 | 22.3788 | 0.95–1.04 | 26–33% |
| Test Region 7 | 21.1410 | 0.82–0.95 | 22–30% |

*The estimates come from applying Figures 5.13 and 5.14 to their misfit angles. Our seven interseismic regions yield $HR$ estimates more compatible with 1.25 than 1.75. It is possible that the Southern California parameterization of $HR$ in Figure 5.8 is elevated to 1.75 by the inclusion of aftershock data. Indeed, the curve for Southern California (Figure 5.8) begins to maximize at an angle that is compatible with $HR = 1.25$, then increases again to an angle compatible with $HR = 1.75$. Our guess is the initial flattening is background seismicity, and the final maximum is due to aftershock data. It would be interesting to have the average focal mechanism difference as a function of distance recalculated for them separately.*

**References**

Becker, T. W., et al. (2005), Constraints on fault slip rates of the southern Califronia plate boundary from GPS velocity and stress inversions, *Geophysical Journal International*, *160*, 634–650.

Ben-Zion, Y., et al. (2003), Large earthquake cycles and intermittent criticality on heterogeneous faults due to evolving stress and seismicity, *Journal of Geophysical Research*, *108*, ESE 1–21.

Hardebeck, J. L. (in review, 2006), Homogeneity of small-scale earthquake faulting, stress and fault strength, *Bulletin of the Seismological Society of America*.

Hardebeck, J. L., and P. M. Shearer (2003), Using S/P amplitude ratios to constrain the focal mechanisms of small earthquakes, *Bulletin of the Seismological Society of America*, *93*, 2434–2444.

Heaton, T. H. (2006, in preparation), Scale dependence of the strength of the Earth's crust.

Michael, A. J. (1984), Determination of stress from slip data: Faults and folds, *Journal of Geophysical Research-Solid Earth*, *89*, 11517–11526.

Michael, A. J. (1987), Use of focal mechanisms to determine stress: A control study, *Journal of Geophysical Research-Solid Earth*, *92*, 357–368.

Scholz, C. H. (1990), *The Mechanics of Earthquakes and Faulting*, Cambridge University Press, Cambridge.